Photocatalytic methane conversion over metal oxides：Fundamentals，achievements，and challenges

JIANG Wenbin[1], LOW Jingxiang[1], QIU Chang[1], LONG Ran[1*], XIONG Yujie[1,2*]

1. *Hefei National Laboratory for Physical Sciences at the Microscale，Collaborative Innovation Center of Chemistry for Energy Materials（iChEM），School of Chemistry and Materials Science，and National Synchrotron Radiation Laboratory，University of Science and Technology of China，Hefei 230026，China；*
2. *Institute of Energy，Hefei Comprehensive National Science Center，Hefei 230031，China*
Corresponding author：longran@ustc.edu.cn；yjxiong@ustc.edu.cn

Abstract：With the rapid development of combustible ice and shale gas mining technology, the reserve of methane (CH_4) has been growing abundant. Therefore, there is a paradigm shift, where CH_4 is not seen only as a hydrocarbon fuel, but also as carbon feedstocks for synthesizing various value-added chemicals. However, the conventional CH_4 conversion technology, especially steam reforming of methane, normally requires extensive energy input due to the extremely stable bonding of CH_4. To this end, photocatalysis, which can break the thermodynamic barrier of CH_4 conversion, has been known as a promising candidate for reaching large-scale CH_4 conversion under ambient condition. In the photocatalytic CH_4 conversion researches, metal oxides have been extensively investigated mainly due to their high oxidation capability. In this review, a discussion is first given on the fundamentals of CH_4 conversion and the advantages of metal oxides in such a reaction. Then the development of metal oxides-based photocatalysts in various CH_4 conversion reactions is reviewed, including total oxidation of methane (TOM), partial oxidation of methane (POM), dry-reforming of methane (DRM), non-oxidative coupling of methane (NOCM), lattice oxygen mediated oxidative coupling of methane (LOCM) and so on. Finally, the opportunities of metal oxides-based photocatalytic CH_4 conversion along with the challenges are summarized.

Keywords：photocatalysis; methane conversion; metal oxides; surface reaction; selectivity

CLC number：O643.36　　　　**Document code**：A

1　Introduction

Methane, as a major component in natural gas, combustible ice and shale gas, has been extensively used in the fuel industry as well as power generation[1-4]. Although it has been proven to be an ideal energy carrier due to its largest heat generation relative to the CO_2 combustion among all the hydrocarbon compounds, its relatively simple chemical structure limits its energy density (0.0378 $MJ \cdot L^{-1}$), which is far lower than most of the commercial hydrocarbon fuels such as gasoline (34.2 $MJ \cdot L^{-1}$) and diesel fuels (38.6 $MJ \cdot L^{-1}$)[5]. Fortunately, CH_4 is also an ideal building block for various chemical compounds, widening its potential in industrial applications[6-10]. Yet, such a CH_4 conversion technology remains underdeveloped due mainly to its extremely stable C—H bond, with dissociation energy of 440 $kJ \cdot mol^{-1}$ at 298 K. In this case, high temperature is commonly required to break the C—H bond and initiate the CH_4 conversion reaction. Currently, the CH_4

conversion is industrially realized through steam reforming of methane (SRM) with an input temperature higher than 700 °C[11-12]. Apart from its obvious shortcoming of high energy consumption, the high input temperature can also cause severe coke deposition, leading to a low CH_4 conversion efficiency ($< 50\%$). Therefore, to achieve a practical application of the CH_4 conversion, it is critical to develop an advanced CH_4 conversion technology from both low energy consumption and high efficiency points of view.

In this regard, various technologies, including thermocatalytic[13-16], electrocatalytic[17-18] and photocatalytic CH_4 conversions[19-22], have been proposed for substituting the obsolete SRM[23-25]. Photocatalysis, which requires only solar energy as the energy input, has shown great promise in CH_4 conversion[19-20]. Typically, a photocatalytic process can not only promote the downhill reactions, but also enable uphill reactions even under ambient temperature (Fig. 1(a)), because the incident photoenergy could compensate the positive

Gibbs free energy of the reaction[2]. Specifically, photogenerated charge carriers with sufficient redox potential can break the thermodynamic limitation, enabling the CH_4 conversion to proceed through a redox reaction. Moreover, under moderate conditions, the above-mentioned coke deposition problems can be greatly suppressed. Conventionally, the photocatalytic CH_4 conversion can be classified into five main groups including total oxidation of methane (TOM), partial oxidation of methane (POM), dry-reforming of methane (DRM), non-oxidative coupling of methane (NOCM) and lattice oxygen mediated oxidative coupling of methane (LOCM). By employing these strategies, various valuable compounds such as ethane, ethylene and ethanol (Fig. 1(b)), have been proven viable to be produced using CH_4 as the building block, suggesting its bright future for fulfilling the demand in the chemical industry.

Over the past several decades, the fast advancement of the photocatalytic CH_4 conversion has ignited the development of various photocatalysts such as metal oxides[20,26], metal nitrides[27] and non-metal-based semiconductors[28-29]. Among them, metal oxides have been the most widely studied photocatalysts for such a fascinating technology. Generally, the metal oxides normally have a superior oxidation ability, allowing them to convert the CH_4 into various target C_{2+} compounds. In addition, their cheapness and easy-tuned properties endow them with wide opportunities in photocatalytic CH_4 conversion. Furthermore, they could also be easily coupled with other materials such as noble metals, semiconductors and metal-organic frameworks, which realizes specific functions in photocatalytic CH_4

conversion such as extended light absorption range, improved photogenerated charge carrier separation and enhanced product selectivity. Therefore, the development of efficient metal oxide photocatalysts is expected to push forward the advancement of the photocatalytic CH_4 conversion for reaching its large-scale applications.

In light of the recent success of metal oxides in photocatalytic CH_4 conversion, this review aims at providing an overview of the current development and achievement of metal oxides in photocatalytic CH_4 conversion. We first summarize and discuss various photocatalytic CH_4 conversion strategies from the viewpoint of theoretical principles. Then we give some comments on the advantages and superiorities of the metal oxides in the photocatalytic CH_4 conversion. Furthermore, we discuss the applications of various metal oxides in photocatalytic CH_4 conversion. Finally, a summary and future prospects of metal oxides in photocatalytic CH_4 conversion are given. We expect that this review could provide some insight and guidelines for future researchers in this field, accelerating the development of photocatalytic CH_4 conversion.

2 Fundamentals of photocatalytic methane conversion

In a typical photocatalytic CH_4 conversion reaction, the activity and selectivity are two fundamental concerns evaluating the performance of a photocatalytic system. For the activity, the cleavage of the first C—H bond of CH_4 is commonly known as its rate-determining step (Fig. 2(a)). Generally, the hydrogen atom in CH_4 can be regarded as the combination of a proton and an electron (H ≡ H^+ + e^-). Therefore, the cleavage of the C—H
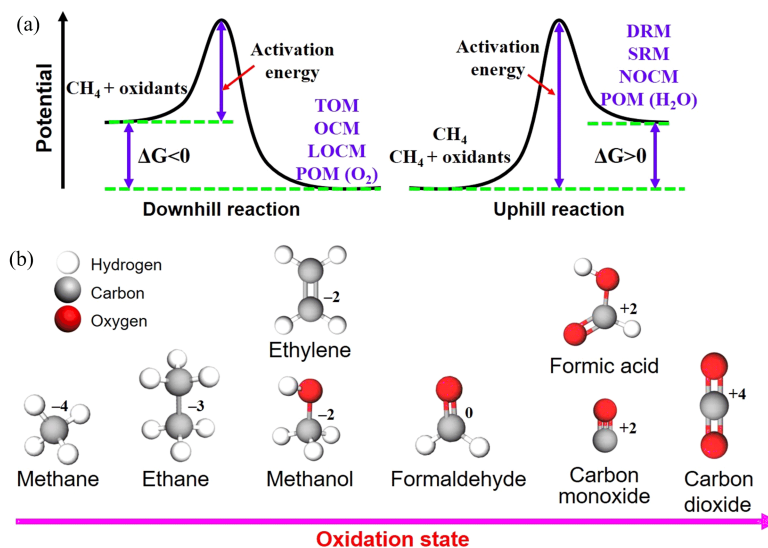

Fig. 1 (a) Schematic illustration for the downhill and uphill photocatalytic methane conversion reactions. (b) Common products for photocatalytic methane conversion and corresponding oxidation state.
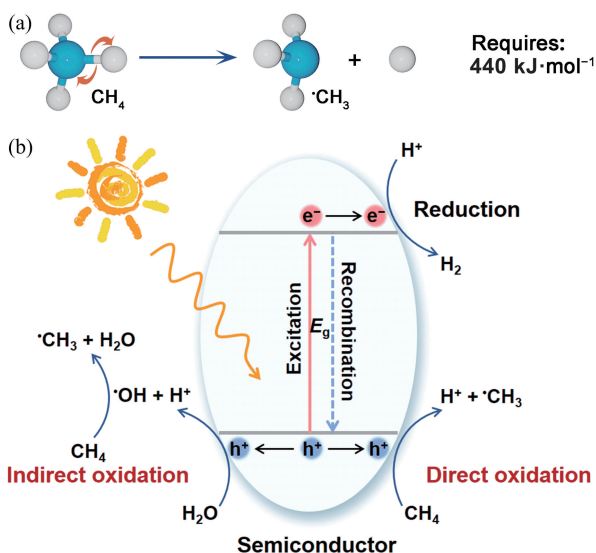
Fig. 2　Schematic illustration of the (a) CH_4 dissociation process and (b) photo-driven CH_4 oxidation process.

bond can be achieved with the presence of electrophilic species (i.e., Lewis acid). In other words, the CH_4 can be oxidized into methyl radicals ($·CH_3$) by accepting the photogenerated holes with sufficient oxidation potential. According to the nature of different photocatalysts and the reaction environments, the cleavage of the C—H bond through photogenerated holes can be achieved via either direct or indirect pathways (Fig. 2(b)). For the ease of understanding, we take metal oxide as an example to interpret these two dissociation pathways of CH_4. Upon light excitation, the photogenerated holes tend to accumulate on the O atoms of metal oxides, creating photogenerated holes-enriched lattice oxygen atoms (O^- centers). For the direct pathway, the O^- centers can directly abstract the H atom from CH_4, generating surface hydroxyl groups and $·CH_3$ radicals. For the latter, the photogenerated holes first react with adsorbate (e.g., water) on the photocatalyst surface to generate electrophilic radicals (e.g., hydroxyl radicals ($·OH$)), which can subsequently oxidize CH_4 into $·CH_3$. It is worth mentioning that the O^- or $·OH$ species assisted C—H bond activation reaction is normally an exothermic process and has low activation energy, enabling the CH_4 conversion reaction to perform under moderate conditions.

　　Another key performance indicator in photocatalytic CH_4 conversion is the product selectivity. Basically, upon the first C—H bond activation, the generated $·CH_3$ possibly undergo various reaction pathways, mainly according to the reaction conditions (see Tab. 1). Conventionally, oxygen (O_2), as a superior oxidant, has been extensively employed as a sacrificial agent for photogenerated electrons to promote the hole-assisted

CH_4 conversion process, accompanied by the generation of reactive oxygen radicals. Under this circumstance, the $·CH_3$ in the reaction system preferentially reacts with the reactive oxygen radicals, leading to the over-oxidation of CH_4 into CO_2 (TOM, Tab. 1, Entry 1). If CO_2 is introduced as a mild oxidant to replace O_2, the reaction product turns to CO (DRM, Tab. 1, Entry 4). If the reaction is carried out in the absence of oxygen element, the $·CH_3$ can be well preserved and further coupled and transformed into ethane (C_2H_6) through the self-coupling process (NOCM, Tab. 1, Entry 5). Beyond that, the $·CH_3$ may also combine with $·OH$ radicals to produce methanol if the water is presented in the reaction system (POM, Tab. 1, Entry 8). Apart from the reaction conditions, the characteristics of the photocatalyst have also been reported to have a significant impact on product selectivity according to their band structure, surface status, oxidation ability, defect density and so on. Therefore, a lot of hydrocarbon and oxygenate compounds have been proven viable to be produced through photocatalytic CH_4 conversion (see Tab. 1, Entry 11~17).

3　Advantages of metal oxides

Metal oxides represent the largest family in heterogeneous catalysts[30-33]. They have been extensively applied in various industrial catalytic processes, such as methanol conversion, propene conversion and ethanol conversion, as oxide catalysts possess superior oxidation capability, wide variety, high stability and intriguing physicochemical properties[34-37]. The application of the metal oxides in photocatalysis can be traced back as early as 1972, when Fujishima and Honda utilized TiO_2 as photocatalysts for initiating the water splitting reaction[38]. Since then, metal oxides have demonstrated their superiority to be employed in various photocatalytic applications[39-44]. In this section, we will discuss the reason why the metal oxides can be an effective photocatalyst for the CH_4 conversion reaction.

3.1　Oxidation ability

As mentioned in the previous section, the high oxidation capability of a semiconductor is the prerequisite for the conversion of CH_4 into various valuable compounds. Typically, for initiating the CH_4 conversion, a semiconductor should own a valence band more positive than the redox potential of $·CH_3/CH_4$ (1.75 V vs. normal hydrogen electrode (NHE)). Fortunately, most of the metal oxides are outstanding oxidation semiconductors with a very positive valence band level (Fig. 3). Therefore, the band structures of the commonly available metal oxides can offer sufficiently high oxidation

Tab. 1 Photocatalytic conversion of CH_4 to various products under different reaction conditions.

Entry	Reactions	Chemical equations
(1) Methane conversion to CO_2		
1	Total oxidation of methane (TOM)	$CH_4 + 2O_2 \rightarrow CO_2 + 2H_2O$
2	Steam reforming of methane (SRM)	$CH_4 + 2H_2O \rightarrow CO_2 + 4H_2$
(2) Methane conversion to CO		
3	Partial oxidation of methane (POM) to CO	$2CH_4 + 3O_2 \rightarrow 2CO + 4H_2O$
4	Dry-reforming of methane (DRM)	$CH_4 + CO_2 \rightarrow 2CO + 2H_2$
(3) Methane conversion to ethane (coupling)		
5	Non-oxidative coupling of methane (NOCM)	$2CH_4 \rightarrow C_2H_6 + H_2$
6	Oxidative coupling of methane (OCM)	$4CH_4 + O_2 \rightarrow 2C_2H_6 + 2H_2O$
7	Lattice oxygen(O_L) mediated OCM (LOCM)	$4CH_4 + 2O_L \rightarrow 2C_2H_6 + 2H_2O + 2O_v$
		$2O_v + O_2 \rightarrow 2O_L$
(4) Methane conversion to CH_3OH		
8	POM to CH_3OH	$CH_4 + H_2O \rightarrow CH_3OH + H_2$
9	Oxidation by hydrogen peroxide	$CH_4 + H_2O_2 \rightarrow CH_3OH + H_2O$
10	Oxidation by oxygen	$2CH_4 + O_2 \rightarrow 2CH_3OH$
(5) Methane conversion to other products		
11	Dehydroaromatization	$6CH_4 \rightarrow C_6H_6 + 9H_2$
12	To aldehyde	$CH_4 + O_2 \rightarrow HCHO + H_2O$
13	To ethanol	$2CH_4 + H_2O \rightarrow C_2H_5OH + 2H_2$
14	To ethylene	$2CH_4 + 2CO_2 \rightarrow C_2H_4 + 2CO + 2H_2O$
15	To acetic acid	$CH_4 + CO_2 \rightarrow CH_3COOH$
16	To acetone	$2CH_4 + CO_2 \rightarrow CH_3COCH_3 + H_2O$
17	To amino acids	$2CH_4 + NH_3 + 2H_2O \rightarrow H_2NCH_2COOH + 5H_2$
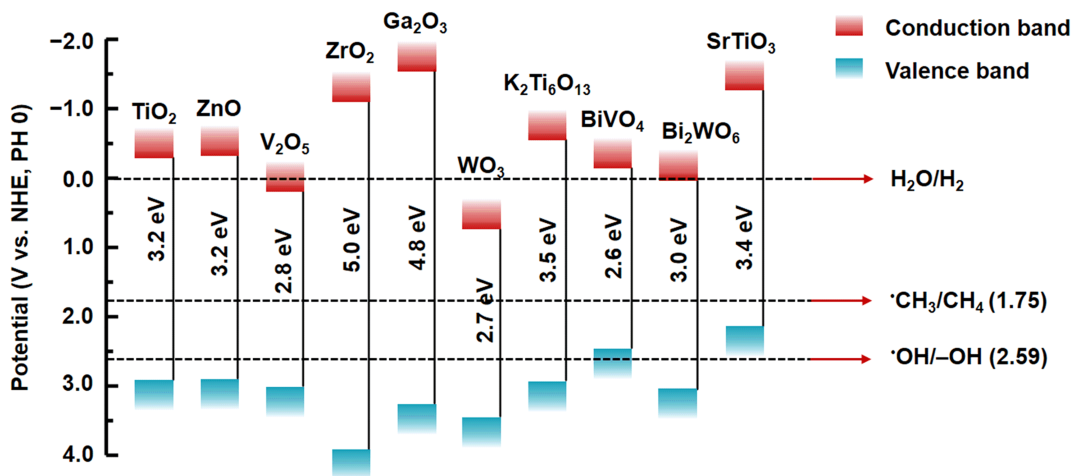
Fig. 3 Schematic illustration of the band structures of common metal oxides for photocatalytic CH_4 conversion.

potentials for the generation of both $\cdot CH_3$ and $\cdot OH$. Moreover, such a high oxidation capability enables the production of a variety of valuable hydrocarbon compounds by simply tuning the properties of metal oxides or reaction conditions, allowing a wide possibility for the metal oxide-based photocatalyst in CH_4 oxidation. It should be noted here that the high oxidation ability of the metal oxides could be a double-edged sword for the photocatalytic CH_4 conversion. Specifically, it could lead to the overoxidation of $\cdot CH_3$ into low-value CO_2. Therefore, various techniques have been performed to precisely control oxidation degree of the resultant products during the photocatalytic CH_4 conversion using metal oxides[20,45]. On the other hand, most of the metal oxides are wide-bandgap semiconductors, absorbing only UV light, which accounts for only 5% in solar light. Fortunately, this limitation can be well tackled by several strategies, such as complexing with narrow-bandgap semiconductors and loading plasmonic metal nanoparticles with strong absorption to visible light[46].

3.2 Metal-methyl interaction

On the metal oxides, the intrinsic presence of metal sites can be a natural promoter for CH_4 conversion. It has been reported that the metal sites on some metal oxides, such as ZnO, Cr_2O_3 and Ga_2O_3, exhibit strong interactions with the methyl moiety of CH_4[47-49]. The existence of these metal-methyl interactions can help polarize the adsorbed CH_4 molecule (Fig. 4 (a)), promoting the cleavage of CH_4 to generate $\cdot CH_3$. Such metal-methyl interactions may be also found on some other metal oxides when their sizes are reduced to cluster or atomic level, due to the existence of abundant coordinatively unsaturated (CUS) metal atoms, which could act as active sites to interact with methyl moiety of CH_4[50-51]. Apart from those features, the adsorption of the generated $\cdot CH_3$ on the metal sites can assist suppressing their reactivity, thereby enhancing their possibility to be coupled into C_2H_6 or slightly oxidized into CH_2, which could be subsequently coupled to form C_2H_4. Clearly, the metal-methyl interaction is one of the keys to achieving highly efficient and selective CH_4 conversion on metal oxides.

3.3 Lattice oxygen reactivity

As we have stated earlier, the photocatalytic CH_4 conversion reaction normally requires the introduction of oxidants such as O_2 for facilitating the cleavage of the stubborn C—H bonds. Yet, the use of oxidants is normally accompanied by the problems of overoxidation[52-55]. In this regard, the lattice oxygen on the metal oxides provides a viable substitution for the external oxidants (Fig. 4 (b)). In detail, upon light irradiation, the photogenerated holes-enriched lattice

oxygen atoms can be utilized for capturing the hydrogen atom from CH_4, generating $\cdot CH_3$ and H^+. Upon C—H bond cleavage of CH_4, if the photogenerated electrons on the metal oxides have sufficient reduction potential (0 V vs. NHE), H_2 can be produced through the reduction of H^+. In contrast, if the reduction potential is insufficient, H^+ will remain on the lattice oxygen, forming hydroxyl groups on the surface of metal oxides. Eventually, water can be formed through dehydration of two neighboring hydroxyl groups, leaving oxygen vacancies on the surface of metal oxides. Simultaneously, the photogenerated electrons reduce metal cations to a lower valence state. To sustain the reaction, the reduced metal oxide can then be reoxidized by seizing oxygen atoms from O_2, CO_2, or water, according to the reaction atmosphere. Clearly, following such a pathway, metal oxides can supply reactive lattice oxygens to facilitate the CH_4 conversion, which is analogous to the Mars-van Krevelen mechanism. In some sense, the lattice oxygen can be regarded as a mild oxidant compared to O_2, avoiding the overoxidation of CH_4 on the metal oxides.

    Overall, the unique advantages of metal oxides are beneficial for highly active and selective CH_4 conversion. The photogenerated holes with strong oxidation ability on metal oxide can break the C—H bond of CH_4 and initiate the reaction. In the meantime, the metal sites on the metal oxides can interact with the methyl moiety for assisting the activation of the C—H
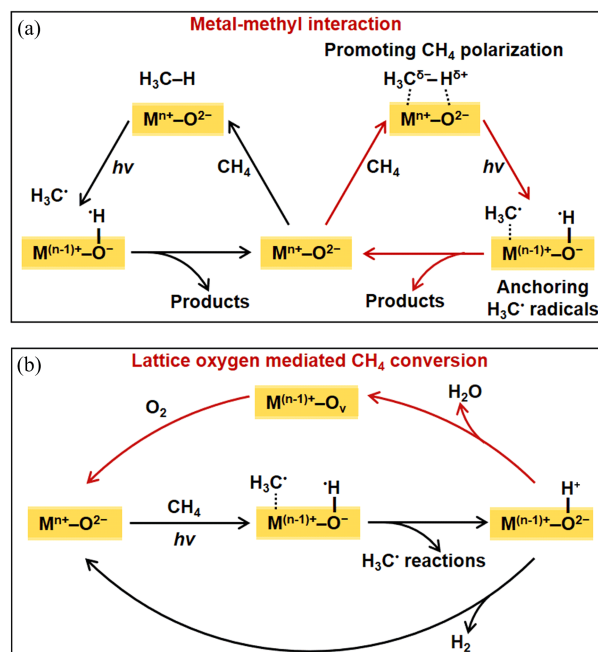

Fig. 4 Schematic illustration of (a) the role of metal-methyl interaction in promoting CH_4 conversion and (b) the lattice oxygen-mediated reaction pathways. M: metal. O_v: oxygen vacancy.
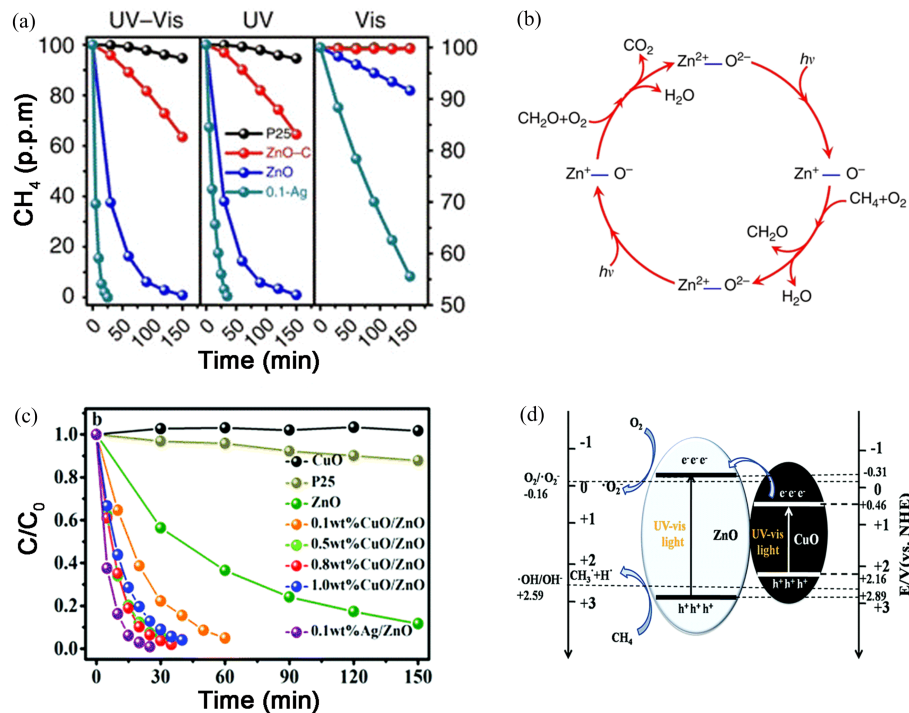
Fig. 5 (a) Comparison of the photocatalytic TOM performance of the commercial TiO_2(P25), commercial ZnO (ZnO-C), ZnO, and 0.1 wt % Ag loaded ZnO (0.1-Ag) under different light irradiation conditions. (b) Schematic illustration for the photocatalytic TOM over Ag/ZnO. (a) and (b) are reproduced with permission from Ref.[61]. Copyright 2016, Springer Nature. (c) Comparison of the photocatalytic TOM performance of the CuO, commercial TiO_2(P25), 0.1 wt% Ag loaded ZnO (0.1wt% Ag/ZnO), and ZnO loaded with different CuO contents including, 0 (ZnO), 0.1 wt (0.1wt% CuO/ZnO), 0.5 wt (0.5wt% CuO/ZnO), 0.8 wt (0.8wt% CuO/ZnO) and 1.0 wt (1.0wt% CuO/ZnO) under full-spectrum irradiation. (d) Schematic illustration for the photocatalytic TOM mechanism over CuO/ZnO. (c) and (d) are reproduced with permission from Ref.[62]. Copyright 2019, The Royal Society of Chemistry.

bond, and stabilize the generated $\cdot CH_3$ for subsequent reactions. More importantly, the lattice oxygen of metal oxide can be directly utilized as a mild oxidant for selective CH_4 conversion. Given these advantages, metal oxides can not only serve as a light absorber to provide highly oxidative photogenerated holes, but also as the active sites for CH_4 conversion.

4 Achievements in photocatalytic methane conversion

4.1 Total oxidation of methane for CO_2 production

Total oxidation of methane, as its name indicates, is complete oxidation of the CH_4 into CO_2. Although the resultant product is low-value, the TOM is the most easily achieved reaction for photocatalytic CH_4 conversion as long as the photocatalysts and oxidants with strong oxidation capability are employed. The success in the photocatalytic TOM has been proven to be a valuable guideline for the other photocatalytic CH_4 conversion reactions to obtain value-added compounds. Typically, the TOM reaction is carried out using O_2 as an oxidant in the gas phase (Tab. 1, Entry 1)[56-60]. For example, Yi and co-workers prepared the Ag/ZnO for photocatalytic TOM (Fig. 5(a))[61]. Attributed to the intriguing surface plasmon resonance (SPR) effect

induced by Ag nanoparticles for extending the light absorption range and promoting the photogenerated charge carrier separation of ZnO, the optimized Ag/ZnO photocatalyst achieved a high quantum yield of 8% at wavelengths <400 nm, demonstrating its superior CH_4 conversion performance. Based on the electron paramagnetic resonance (EPR) and in situ infrared spectra (Fig. 5(b)), the major role of photogenerated charge carriers in CH_4 oxidation can be revealed. In detail, upon the light irradiation, the electron in oxygen atom transfers to Zn atom, forming a $Zn^+ - O^-$ pair on ZnO. Then the reactants, including CH_4 and O_2, were oxidized and reduced, respectively, leading to the formation of $\cdot CH_3$ and $O_2^{\cdot -}$. Subsequently, these produced $\cdot CH_3$ and $O_2^{\cdot -}$ could be coupled to produce CH_2O, followed by its transformation into CO_2 with water as the by-product. Furthermore, the same research group reported that depositing a tiny amount of CuO on the surface of ZnO can also achieve a performance comparable to that of Ag/ZnO (Fig. 5(c))[62]. The narrow-bandgap semiconductor CuO functions to expand light absorption and promote charge carrier generation. Mechanistic studies suggested that the reaction was also achieved through $O_2^{\cdot -}$ (Fig. 5(d)), further confirming the roles of the O_2 as an important oxidant for accelerating the TOM.
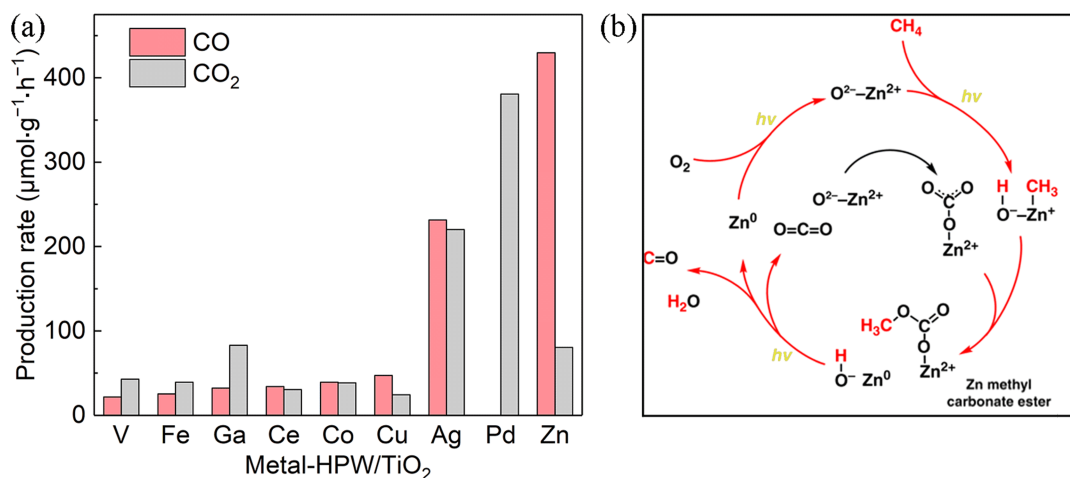
Fig. 6 (a) Comparison of the photocatalytic partial oxidation of methane for CO production using various metal-modified HPW/TiO$_2$ under 6 h of light irradiation. (b) Schematic illustration for the proposed mechanism for photocatalytic partial oxidation of methane for CO production on Zn-HPW/TiO$_2$. Reproduced with permission from Ref.[72]. Copyright 2019, Springer Nature.

4.2 Dry-reforming and partial oxidation of methane for CO production

After confirming the viability of the CH$_4$ conversion through photocatalytic TOM using O$_2$ as oxidants, a question innately arises as to whether it is possible to control the oxidation degree of the reactants during the CH$_4$ conversion to avoid its overoxidation into low-value CO$_2$. Clearly, this aim can be reached by substituting O$_2$ with CO$_2$, a weaker oxidant (DRM, Tab. 1, Entry 4) to retard the oxidation reaction. Generally, DRM is a typical uphill reaction that suffers from thermodynamic limitations and high energy requirements[63-66]. To carry out the DRM, the photocatalyst should have suitable valence and conduction band positions to satisfy both CO$_2$ reduction and CH$_4$ oxidation reactions. In this regard, wide-bandgap metal oxides ($>$3.0 eV) such as TiO$_2$, ZnO, Ga$_2$O$_3$, ZrO$_2$, and MgO are commonly chosen for this reaction[67-70]. In addition to light illumination, the reactions are commonly carried out at elevated temperatures due to the stable bonding of both CO$_2$ and CH$_4$; otherwise, only traces of CO and H$_2$ could be detected. For instance, Yoshida and co-workers discovered that mild thermal energy (200~400 °C) was required to reach a noticeable production of CO and H$_2$ through photocatalytic DRM using Ga$_2$O$_3$[69]. However, the CH$_4$ conversion efficiency in their work at 200 °C and 3 h of light irradiation is relatively low (0.27%). To address this issue, Miyauchi and co-workers recently fabricated an SrTiO$_3$ supported Rh photocatalyst[71]. The catalyst exhibited a stoichiometric production of CO and H$_2$ with a rate of approximately 54 mmol · g^{-1} · h^{-1} under the UV light irradiation without external heat input. Based on isotope labeling studies, this result was attributed to the participation of the lattice oxygen during the reaction. Specifically, upon light irradiation, photogenerated holes-enriched lattice oxygen oxidized CH$_4$ to produce CO and H$_2$, accompanied by the generation of oxygen vacancies. Then the photogenerated electrons were transferred to Rh sites, reducing the CO$_2$ to CO, concomitant with the regeneration of lattice oxygen of SrTiO$_3$.

Other than substituting the oxidants, the control over oxidation degree can be reached by manipulating the surface status of the photocatalysts to weaken the oxidation reaction on their surface and reach POM. For example, Khodakov and co-workers fabricated a series of metal-heteropolyacid-titania composites (M — HPW/TiO$_2$, M=V, Fe, Ga, Ce, Co, Cu, Ag, Pd, Zn) to employ the metal species for avoiding the generated methyl species from overoxidation during the CH$_4$ conversion[72]. Among them, the Zn-HPW/TiO$_2$ photocatalyst with optimized Zn content exhibited the highest CO production of 429 μmol · g^{-1} · h^{-1} with a selectivity of more than 84% (Fig. 6(a)) in the presence of CH$_4$ and O$_2$. This system achieved such a selectivity because the HPW-stabilized highly dispersed Zn species can easily react with the atmosphere O$_2$ to form Zn^{2+} — O^{2-} pairs, preventing the transformation of O$_2$ into highly reactive O$_2^{\cdot-}$ (see Fig. 6(b)). Such Zn^{2+} — O^{2-} pairs own similar behaviors to the ZnO, in which these Zn^{2+} — O^{2-} pairs can be photoexcited under light irradiation, forming Zn$^+$ — O$^-$ pairs on its surface. Then the first C—H bond of CH$_4$ can be broken by these Zn$^+$ — O$^-$ pairs, forming a Zn-methyl species (Zn stabilized ·CH$_3$) and a surface hydroxyl group. The Zn-methyl species could then combine with nearby Zn carbonate to produce Zn methyl carbonate ester, which was further decomposed into CO, H$_2$O, and Zn carbonate species under the light irradiation. Simultaneously, the Zn species can be recovered and readily utilized for the next cycle of the
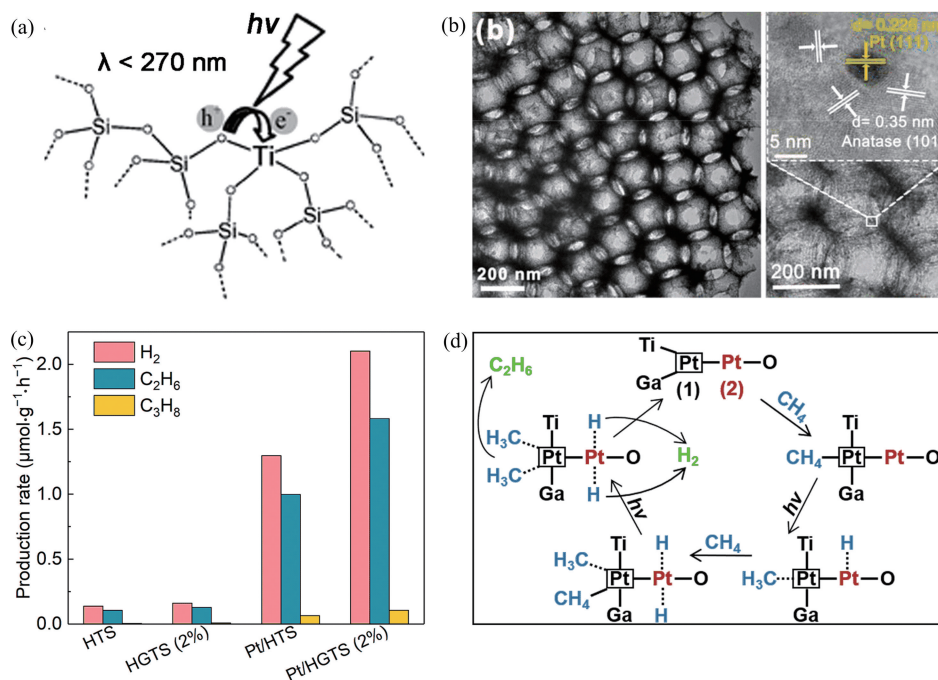
Fig. 7 (a) Schematic illustration of the photoexcitation process over silica-supported dispersed Ti-O tetrahedral sites. Reproduced with permission from Ref.[2]. Copyright 2008, The Royal Society of Chemistry. (b) Transmission electron microscopy (TEM) images of Pt/ HGTS (2%). (c) Comparison of the photocatalytic NOCM performance over highly-ordered TiO_2-SiO_2 composites (HTS) and Pt-modified Ga-doped HTS (HGTS) under 4 h of light irradiation. (d) Photocatalytic NOCM reaction pathways over Ga and Pt co-modified HTS. (b)～ (d) are reproduced with permission from Ref.[77]. Copyright 2019, American Chemical Society.

CH_4 conversion reaction. This work suggested that the proper control of the surface status of a photocatalyst is vital for controlling the O_2 activation process and thus the final products of the photocatalytic CH_4 conversion.

The above-mentioned works confirmed that the proper control of the oxidation degree during the CH_4 conversion can be a significant strategy for manipulating product selectivity. Yet, their obtained product is normally CO, which only has a slightly higher value than CO_2. In this regard, Tang and co-workers reported a unique strategy for further suppressing the oxidation degree of the CH_4 to realize the oxidative coupling of methane (OCM, Tab. 1, Entry 6) and obtain C_{2+} compounds (C_2H_6 and C_2H_4) in the presence CH_4 and O_2. In detail, they loaded the CuO_x on the TiO_2, to guide the photogenerated hole migration from TiO_2 to CuO_x with weak oxidation capability. Moreover, the Pt nanoparticles were also loaded on TiO_2/CuO_x to enhance the photogenerated charge carrier separation efficiency. As a result, the photocatalytic C_{2+} compound production rate of optimized Pt and CuO_x co-modified TiO_2 reached 6.8 μmol · h^{-1} with a selectivity of 60%, far exceeding that of the pristine TiO_2. In this case, the key is the use of CuO_x with weak oxidation capability that could retard the CH_4 oxidation reaction, prohibiting the overoxidation of CH_4 into CO_2. This work suggested that the control of the oxidation degree during the photocatalytic CH_4 conversion could obtain the products

beyond CO, greatly extending the potential of this fascinating technology. Nevertheless, reports on photocatalytic POM/OCM toward the high-value C_{2+} products remain scarce. Therefore, the follow-up work in this respect is highly sought after.

4.3 Non-oxidative coupling of methane for C_2H_6 production

The NOCM reaction is a CH_4 conversion reaction that directly converts CH_4 into C_2H_6 and H_2 (Tab. 1, Entry 5) without using any external oxidants[2]. From the thermodynamic perspective, the change of Gibbs free energy (ΔG_{298K}^0) for NOCM is positive (68.6 kJ · mol^{-1}). Therefore, NOCM can hardly proceed at room temperature. With the aid of the photocatalytic reaction, such a difficult uphill reaction can be reached by consuming the photogenerated charge carriers with strong redox capability on the semiconductors. For instance, Yoshida and co-workers reported a series of works using silica- or alumina-supported highly-dispersed metal oxides for the photocatalytic NOCM[73-75]. It was demonstrated that, upon photoexcitation, the photogenerated electrons can transfer from oxygen atoms to metal atoms, leaving photogenerated holes on oxygen atoms (Fig. 7(a)). Then the photogenerated hole-enriched oxygen atom (i.e., O^-) broke the C—H bond of CH_4, initiating the CH_4 conversion. As a result, C_2H_6 and H_2 can be simultaneously produced with the utilization of only

CH_4, photocatalyst and light source. To further enhance the photocatalytic NOCM performance, the same group of researchers developed a SiO_2-Al_2O_3-TiO_2 ternary photocatalyst by introducing two distinct semiconductors onto silica[76]. It was revealed that the silica could allow the metal oxides to disperse uniformly, thus providing enormous amounts of surface active sites for the reaction, while Al_2O_3 and TiO_2 acted as the light absorbers for initiating the photocatalytic reaction. Therefore, the optimized SiO_2-Al_2O_3-TiO_2 achieved a C_2H_6 production of approximately 0.7 μmol $\cdot$ $g^{-1} \cdot h^{-1}$ under the deep UV light ($\lambda < 270$ nm) irradiation. Although C_2H_6 and H_2 can be simultaneously produced with the use of the only CH_4, photocatalyst and light irradiation, these highly dispersed systems suffer from weak light absorption and severe recombination of photogenerated charge carriers.

To further boost the photocatalytic NOCM performance, Zhang and co-workers adopted the Pt to couple with highly ordered TiO_2-SiO_2(HTS) for further enhancing their photocatalytic NOCM performance (Fig. 7(b))[77]. It is discovered that the metallic Pt can act as a superior co-catalyst for spatially separating the photogenerated electron-hole pairs on HTS. After reaching this aim, they further introduced the Ga-doping to tune the valence status of the loaded Pt to extend the function of Pt in this composite. In detail, the Ga doping could cause the formation of cationic Pt for strengthening the dissociation of CH_4. As a result, the optimized Pt and Ga modified HTS (Pt/HGTS) displayed a CH_4 conversion rate of 3.48 μmol $\cdot g^{-1} \cdot h^{-1}$ with a selectivity of 90.1% toward C_2H_6 production (Fig. 7(c)). Yet, it should be always kept in mind that the concentration of the Ga-doping should be controlled because it could cause a decrease in the photogenerated charge carrier separation efficiency. To have a full image of the role of Pt loading and Ga doping, theoretical calculations were also performed, showing that the metallic Pt and Ga-induced cationic Pt could serve as a cationic-anionic pair to promote the polarization of CH_4 molecule (Fig. 7(d)). Upon photo-excitation, the cationic Pt could easily abstract the hydrogen atom from CH_4, forming $\cdot CH_3$, while the metallic Pt stabilized the produced $\cdot CH_3$ for their subsequent transformation into C_2H_6.

Other than boosting the photogenerated charge carrier separation, the optimized surface-active site can also be beneficial for improving photocatalytic NOCM performance. To this context, Chen and co-workers developed a zinc-modified zeolite photocatalyst ($Zn_{0.69}AlSi_{14.8}O_{31.6}$) for photocatalytic NOCM (Fig. 8 (a))[21]. The photocatalyst exhibited a CH_4 conversion rate of 9.8 μmol $\cdot g^{-1} \cdot h^{-1}$ with a C_2H_6 selective of 99.6% under ambient conditions (room temperature, 1 atm, high-pressure Hg lamp). This excellent CH_4 conversion performance was achieved because the Zn cations were uniformly dispersed on the zeolite framework, providing abundant surface-active sites on the photocatalyst. Moreover, the Zn sites with variable valence state (i.e., Zn^{2+} and Zn^+) can serve as a bridge for the charge carrier transfer from the zeolite framework to CH_4 molecule, facilitating the surface reaction on the photocatalyst (Fig. 8(b)).

Such work on the superiority of the metal active sites in enhancing photocatalytic NOCM has encouraged follow-up works to further boost the photocatalytic NOCM performance using Zn-containing metal oxides. For example, Long and co-workers fabricated a porous ZnO nanosheet supported Au for photocatalytic NOCM[78]. Owing to the simultaneous excitation of ZnO inter-band transition and Au SPR under the full spectrum light irradiation, the optimized photocatalyst displayed a C_2H_6 production of approximately 45 μmol $\cdot$ g^{-1} after 4 h of irradiation, concomitant with the production of stoichiometric H_2(Fig. 8(c)). In this case, the CH_4 molecule was oxidized by the photogenerated holes on ZnO, forming the $\cdot CH_3$, which could then be stabilized by the Zn^+ site. Subsequently, this generated $\cdot CH_3$ could combine with another $\cdot CH_3$ to produce C_2H_6 (Fig. 8(d)). More interestingly, it was revealed that the SPR-induced local electric field on Au plays a significant role in boosting the photocatalytic NOCM performance of ZnO, where the local electric field induced by Au could facilitate the photogenerated charge carrier migration for enhancing the surface reaction on the Au-ZnO.

Although it is well studied that the CH_4 conversion is an oxidation reaction, the consumption of electrons during the reaction is an inevitable issue to optimize the photocatalytic NOCM performance. For this reason, Yu et al. established a photocatalytic reaction system combining NOCM with water splitting using Pt loaded TiO_2[79]. The Pt/TiO_2 catalyst with optimized Pt loading achieved an H_2 and C_2H_6 evolution rate of 208.2 μmol $\cdot$ $g^{-1} \cdot h^{-1}$ and 54.4 μmol $\cdot g^{-1} \cdot h^{-1}$, respectively. It was unveiled that water plays dual functions in this photocatalytic system, where it can consume photogenerated electrons to produce H_2 and utilize photogenerated holes to produce $\cdot OH$. $\cdot OH$ can be subsequently utilized to react with CH_4 molecules for generating $\cdot CH_3$. In the meantime, Pt was a bifunctional cocatalyst in this photocatalytic system, where it can act as an active site for H_2 production and also a stabilizing site for $\cdot CH_3$ to allow their subsequent coupling into C_2H_6. Yet, it should be noted that the production of O_2 from H_2O is also unavoidable in this reaction system,
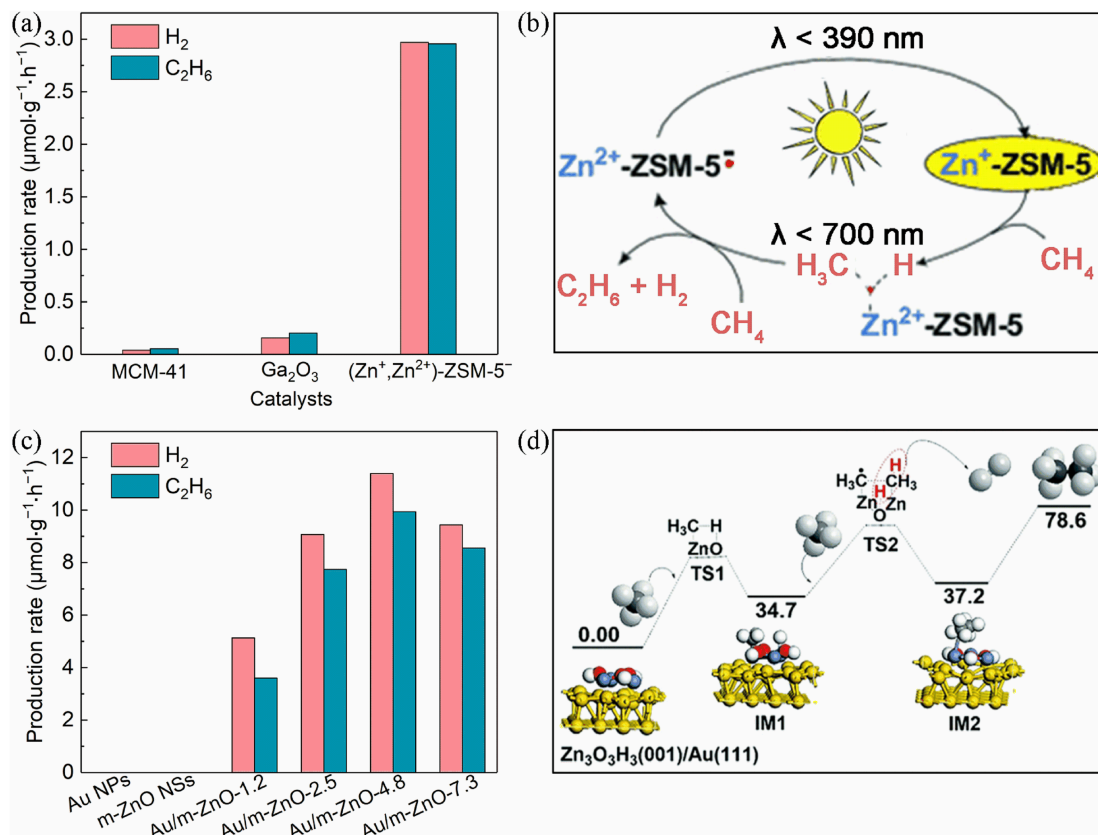
Fig. 8 (a) Comparison of the photocatalytic NOCM performance over MCM‑41, Ga_2O_3, and (Zn^+, Zn^{2+})‑ZSM‑5$^-$ under 8 h of high‑pressure Hg lamp irradiation. (b) Proposed mechanism for photocatalytic NOCM reaction mediated by Zn^+ active sites. (a) and (b) are reproduced with permission from Ref.[21]. Copyright 2011, John Wiley & Sons, Inc. (c) Comparison of the photocatalytic NOCM performance over Au nanoparticles (Au NPs), ZnO (m‑ZnO NSs) and ZnO loaded with different Au contents including 1.2 wt% (Au/m‑ZnO‑1.2), 2.5 wt% (Au/m‑ZnO‑2.5), 4.8 wt% (Au/m‑ZnO‑4.8) and 7.3 wt% (Au/m‑ZnO‑7.3) under 4 h of light irradiation. (d) Relative potential energy surfaces for methane coupling reactions on $Zn_3O_3H_3(001)/Au(111)$. (c) and (d) are reproduced with permission from Ref. [78]. Copyright 2018, The Royal Society of Chemistry.

causing massive CO_2 production. Therefore, the C_2H_6 selectivity would be greatly suppressed in this reaction condition[80].

Based on these examples, it is obvious that the photocatalytic reaction achieves the "impossible" mission. With the aid of the photogenerated charge carriers, the uphill photocatalytic NOCM for C_{2+} compound production was achieved under the ambient condition with photon energy as the only energy input. Nevertheless, the performance of photocatalytic NOCM remains far from satisfactory due to the absence of the oxidants. Therefore, future researches on enhancing the photocatalytic performance of NOCM through materials engineering are highly desired.

4.4 Lattice oxygen mediated oxidative coupling of methane for C_{2+} hydrocarbon production

As mentioned in the previous section, the H atom on CH_4 can be abstracted by the lattice oxygen and subsequently coupled to form H_2O. Due to the participation of the lattice oxygen as the oxygen source,

this CH_4 conversion pathway is known as lattice oxygen mediated oxidative coupling of methane (LOCM). However, this reaction should be distinguished from the conventional OCM reaction[81‑82]. In detail, the C_{2+} products can hardly be formed through OCM reaction due to the utilization of O_2, which could lead to the overoxidation of the reactants into CO_2[45]. In contrast, for the LOCM, the lattice oxygens can be regarded as mild oxidants, which not only assist the CH_4 conversion but also suppress the overoxidation of reactants. Therefore, an impressive photocatalytic CH_4 conversion performance with high selectivity toward C_{2+} compounds can be potentially reached via photocatalytic LOCM.

For example, Chen and co‑workers developed a Ga^{3+}‑modified zeolite (ETS‑10, titanosilicate) catalyst for photocatalytic LOCM[83]. The sample demonstrated a CH_4 conversion rate of 29.8 $\mu mol \cdot g^{-1} \cdot h^{-1}$ with a C_{2+} hydrocarbon product (C_2H_4, C_2H_6, C_3H_6, C_3H_8, C_4H_6 and C_4H_{10}) selectivity of approximately 100%
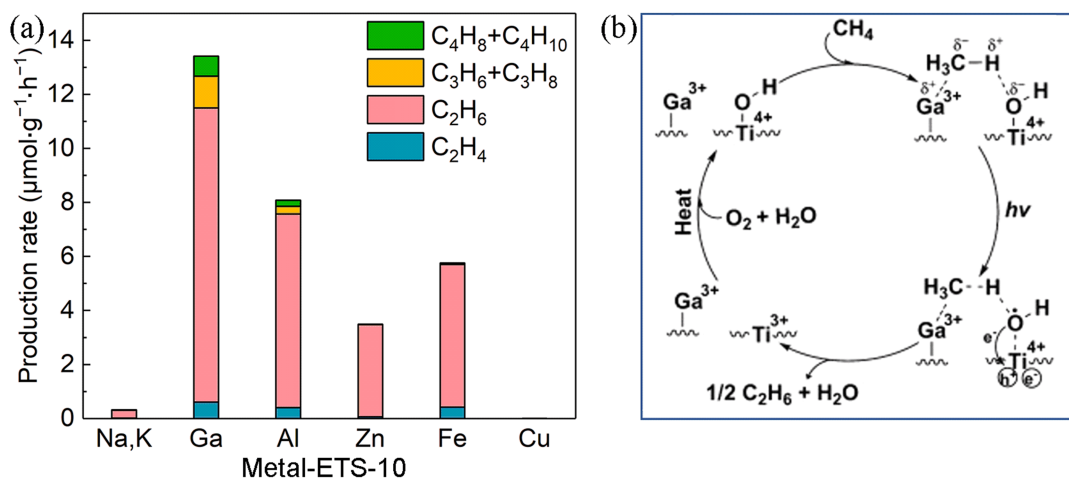
Fig. 9 (a) Photocatalytic methane conversion performance using metal (Ga, Al, Zn, Fe, Cu and Na, K)-modified ETS-10 zeolite samples (ETS-10 = titanosilicate) under 5 h of high-pressure Hg-lamp irradiation. (b) Schematic illustration for the proposed mechanism for photocatalytic methane reaction over Ga^{3+}-modified ETS-10. Reproduced with permission from Ref.[83]. Copyright 2012, John Wiley & Sons, Inc.

after 5 h of UV light irradiation (Fig. 9(a)). This superior photocatalytic CH_4 conversion performance was attributed to the synergistic effect of Ga^{3+} cations and the $Ti—O^{\delta-}H$ groups in the ETS-10 framework (Fig. 9 (b)). More interestingly, C—H symmetric vibration, which is infrared forbidden, can be observed in the Fourier-transform infrared spectra of the prepared samples, due to the polarization of the adsorbed CH_4 molecules by the cationic-anionic pairs formed between Ga^{3+} cation and $O^{\delta-}$ anion. Such a unique polarization of CH_4 molecules is expected to weaken the C—H bonds, and thus enhance the CH_4 conversion efficiency. Therefore, under UV-light irradiation, photogenerated holes-enriched $O^{\delta-}$ sites can easily abstract the H atom from CH_4, forming $\cdot CH_3$, which is subsequently coupled to form hydrocarbon compounds. Concomitantly, the oxygen vacancy will be formed on the ETS-10 due to the consumption of lattice oxygen for the formation of water. Fortunately, the consumed lattice oxygen on the surface $Ti—O^{\delta-}H$ groups could be regenerated by thermal treatment in the presence of O_2 and water at 250 °C for 2 h, sustaining the photocatalytic LOCM reaction.

Apart from the consumption of lattice oxygen on the photocatalyst, the lattice oxygen on the co-catalyst can also be utilized for the proceeding of photocatalytic LOCM. For example, Khodakov and co-workers developed a silver-heteropolyacid-titania (Ag—HPW/TiO_2) composite for LOCM[26]. Generally, TiO_2 and Ag served as light-harvesting centers and surface-active sites for the reaction, respectively, while the HPW played a vital role in enhancing the dispersion of Ag cations (as AgO_x). Then the photocatalytic CH_4 conversion test was performed, showing that the HPW/TiO_2 exhibited negligible CH_4 conversion due to the absence of proper

active sites and oxidants. In contrast, after the introduction of AgO_x species, the photocatalytic performance of the HPW/TiO_2 was momentously improved, displaying a CH_4 conversion rate of 50.1 $\mu mol \cdot g^{-1} \cdot h^{-1}$ with a C_2H_6 production rate of 20.3 $\mu mol \cdot g^{-1} \cdot h^{-1}$ after 7 h of light irradiation. In this system, the lattice oxygen of AgO_x can take part in the CH_4 conversion as an oxidant, facilitating the reaction. Yet, it is worth noting that the lattice oxygen in relatively large AgO_x clusters possessed stronger oxidation ability, leading to enhanced CO_2 production and reduced C_2H_6 selectivity. Similar to the above-mentioned example, the consumption of the lattice oxygen on AgO_x can result in a decrease in photocatalytic performance. Nonetheless, the regeneration of the lattice oxygen on AgO_x was rather simple, in which the metallic Ag nanoparticles could be easily re-oxidized into highly dispersed Ag cations by light irradiation in an air atmosphere.

As demonstrated by these examples, the photocatalytic LOCM reactions commonly display higher CH_4 conversion efficiency than the NOCM reaction, as the LOCM reaction is thermodynamically more favorable. Moreover, compared with the above-mentioned NOCM reaction using water as a promoter, the lattice oxygen assisted CH_4 conversion displays a higher selectivity toward C_2H_6. These examples highlight the great potential of lattice oxygen of metal oxide as a mild oxidant in achieving highly active and selective CH_4 conversion. Nevertheless, the limitation of the photocatalytic LOCM is also pronounced. Specifically, the consumption of lattice oxygen during the reaction can interrupt the stability of the photocatalytic reaction. Therefore, a secondary reaction

is always required to regenerate the lattice oxygen for sustaining the reaction.

4.5 Partial oxidation of methane for CH_3OH production

The partial oxidation of methane into oxygenate products (e.g., methanol, formaldehyde, and formic acid) has long been a topic in CH_4 conversion[84]. In this reaction, an oxidant is indispensable for supplying oxygen atoms to produce oxygenate products. As such, the key to this reaction is to realize an efficient CH_4 conversion while avoiding the overoxidation of reactants in the presence of the oxidant. Typically, the reactions can be carried out in reaction conditions consisting of H_2O or H_2O_2 for the production of $\cdot OH$. Specifically, H_2O can be regarded as the mildest oxidant[85-88], which is expected to be beneficial to the reaction selectivity (Tab. 1, Entry 8). In this regard, Noceti et al. reported La-doped WO_3 photocatalyst with a CH_4 conversion efficiency of 4% under UV light irradiation at a temperature of $\sim 94\ ^\circ C$ and atmospheric pressure[89-90]. In this work, methyl viologen dichloride hydrate (MV) was added as an electron sacrificial agent to consume photogenerated electrons accumulated on WO_3. Therefore, more photocatalytic holes can take part in water oxidation to generate $\cdot OH-$ the key intermediate for converting CH_4 to methanol. Following this line of thought, Villa et al. employed Cu^{2+} and Fe^{3+} as photogenerated electrons scavengers to enhance the production of $\cdot OH$ for promoting methanol production over WO_3 photocatalyst[91]. It was revealed that the use of Cu^{2+} and Fe^{3+} can result in 1.7- and 2.0-fold enhancement in photocatalytic CH_4 conversion performance toward methanol production in comparison with the pristine WO_3. Yet, it should be taken into account that not all the cations are suitable to act as electron scavengers for such a reaction. In detail, they discovered that the introduction of Ag^+ led to a declined performance because Ag^+ could be easily reduced into metallic Ag which then covered the surface of WO_3 and prohibited WO_3 from absorbing incident light.

Although the addition of electron scavenger can significantly promote methanol production, this strategy is not effective from the economic point of view. In this sense, modification of the photocatalyst through surface engineering can be a versatile strategy for simultaneously tuning the photocatalytic activity and selectivity. For instance, Villa et al. enhanced the surface $\cdot OH$ production on the WO_3 through La-doping for photocatalytic CH_4 conversion toward oxygenate compound production[92]. In detail, the La-doping can cause the generation of the oxygen vacancies on WO_3, which is beneficial for the water adsorption and surface $\cdot OH$ production. As a result, compared to pristine WO_3, the La-doped WO_3 exhibited a significant enhancement in methanol production (1.9-fold) and a decrease in CO_2

and C_2H_6 production, suggesting its enhanced selectivity toward methanol production. To evaluate the importance of the $\cdot OH$, they introduced the F^- on the WO_3 to prohibit the formation of the $\cdot OH$ during the photocatalytic CH_4 conversion[93]. After fluorination, the production of methanol using WO_3/F^- was significantly reduced because F^- can prohibit the formation of $\cdot OH$ by allocating their reactive sites on the WO_3. Based on these findings, they discovered that the $\cdot OH$ attached on the surface of WO_3 was certainly responsible for the selective conversion of CH_4 to methanol under light irradiation.

Apart from those, it is well recognized that the decrease in surface acidity on photocatalyst can also lead to an enhancement in the methanol selectivity due to the reduced reactivity of the surface oxygen functional groups for avoiding overoxidation of reactants[92]. To this end, Murcia-López et al. modified the beta-zeolite catalyst with Bi and V (Bi-V-HBET) to reduce its surface acidity[94]. It was discovered that, although pristine zeolite exhibited considerable photocatalytic CH_4 conversion activity, its final products were dominated with CO_2 due to the overoxidation of the reactants (Fig. 10(a)). After the Bi and V co-modification, the Bi-V-HBET displayed a substantially decreased CO_2 production and increased selectivity toward methanol production (from 2.3% to 6.5%). In this case, the presence of Bi and V elements can effectively reduce the number of acidic Al—O units and surface Si—OH groups, resulting in the decreased surface acidity. This inference was also evaluated through the pyridine absorption test, showing that the Bi-V-HBET exhibited a magnificent decrease in surface acidity as compared to pristine beta-zeolite.

Given the different reactivity of the distinct surfaces of a semiconductor, it is expected that the oxidation reactivity on a specific semiconductor can also be tuned by manipulating the exposed ratio of different facets. Recently, Sadtler and co-workers investigated the impact of different morphologies, including bipyramid, thick platelet and thin platelet, on the photocatalytic CH_4 conversion performance of $BiVO_4$[95]. Among them, it was revealed that the bipyramid $BiVO_4$ exhibited the highest methanol production rate of 112 $\mu mol \cdot g^{-1} \cdot h^{-1}$ and a selectivity of 85% after 1 h irradiation at 65 $^\circ C$ (Fig. 10(b)). According to the photodeposition test, photogenerated holes could be extracted from the whole surface of bipyramid $BiVO_4$ (see Fig. 10(c)), while photogenerated electrons were selectivity accumulated on its apexes (see Fig. 10(d)). Such a result suggested that the bipyramid $BiVO_4$ had enormous oxidative surface-active sites, thereby optimizing its CH_4 conversion performance. In contrast, the thick platelets only had small oxidative surface for photogenerated hole accumulation (see Fig. 10(e)), resulting in its low
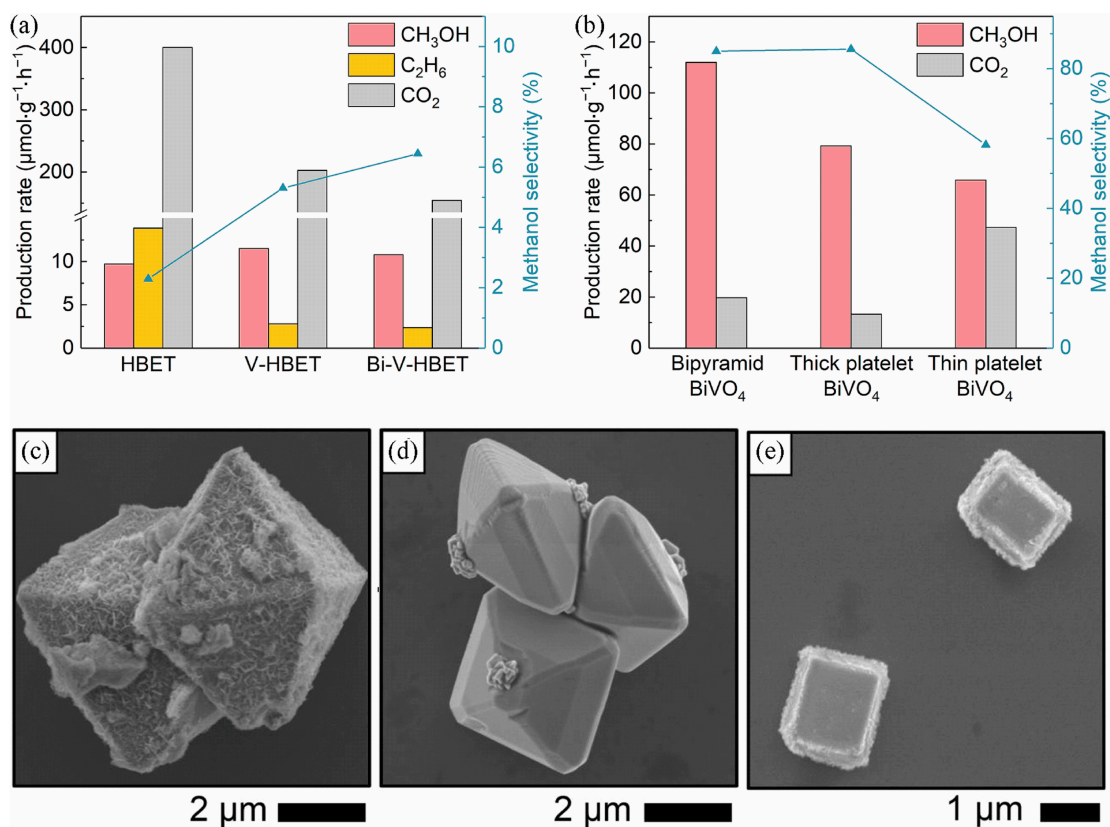
Fig. 10 (a) Comparison of the photocatalytic methane conversion performance over pristine beta-zeolite (HBET), V-modified beta-zeolite (V-HBET), and Bi, V-co-modified beta-zeolite (Bi-V-HBET) samples under 2 h of UVC-visible light irradiation. Reproduced with permission from Ref. [94]. Copyright 2017, American Chemical Society. (b) Comparison of the photocatalytic methane conversion performance of the $BiVO_4$ with different morphologies under 2 h of AM1.5 simulated light irradiation. (c,d) Scanning electron microscope images for photodeposition of manganese oxide (indicator for oxidation site) using $MnSO_4$ as precursor on $BiVO_4$ bipyramid (c) and Au (indicator for reduction site) using $HAuCl_4$ as precursor (d). (e) Scanning electron microscope image for photodeposition of manganese oxide using $MnSO_4$ as precursor on $BiVO_4$ thick platelet. (b) ～ (e) are reproduced with permission from Ref. [95]. Copyright 2018, American Chemical Society.

methanol production. This work demonstrated that the redox surface of a semiconductor should be tuned during the photocatalytic CH_4 conversion using a metal oxide photocatalyst.

Apart from H_2O, H_2O_2 has also been extensively employed as oxidants for guiding the CH_4 conversion into oxygenate compounds (Tab. 1, Entry 9)[96]. Typically, H_2O_2 can simultaneously act as an electron scavenger and a source of ·OH, both of which are beneficial for promoting the activation of CH_4. For example, Tang and co-workers developed a series of metal/metal oxide modified TiO_2 photocatalyst for photocatalytic POM using H_2O_2 as oxidant[20]. The FeO_x/TiO_2 with an optimized FeO_x loading content achieved a methanol production of 1056 $\mu mol \cdot g^{-1}$ with selectivity over 90% after 3 h of light irradiation at 25 °C. Furthermore, the carbon source of the generated methanol was confirmed by isotope labeling experiments using CH_4 with different labelings as reactants. The results showed that the resultant m/z values of the methanol varied from 32 (using $^{12}CH_4$ as reactant) to 33 (using $^{13}CH_4$ as

reactant) with the change of CH_4 labeling, manifesting that the CH_4 was certainly the source of the generated methanol. It should be noted here that the H_2O_2 amount is the key to reaction activity and selectivity; low amount resulted in a substantially declined activity while high amount led to obvious CO_2 production. Specifically, the excess H_2O_2 amount induced the enormous production of O_2 in the photocatalytic system, thereby causing the overoxidation of the reactant into CO_2. Based on the obtained result, they proposed a FeO_x-enhanced methanol production mechanism on the TiO_2. In detail, the presence of FeO_x could assist inhibiting the reduction of O_2 to highly oxidative $O_2^{·-}$, thereby retarding the overoxidation of reactants into CO_2 and promoting the methanol production. Moreover, structural characterization suggested that FeO_x was highly dispersed on the surface of TiO_2 in the form of Fe_2O_3 and FeOOH. Upon light irradiation, the highly dispersed FeO_x species could serve as a bridge to promote the charge transfer from TiO_2 to H_2O_2, resulting

in the enhanced generation of ·OH. Concurrently, CH_4 was activated by photogenerated holes to form ·CH_3, which could then be combined with the ·OH to produce methanol. This strategy has also been adopted and proven to be effective for other semiconductors. Specifically, Yang et al. modified WO_3 with FeO_x and the optimized $FeOOH/WO_3$ sample achieved a methanol production rate of 211 μmol · g^{-1} · h^{-1} with a selectivity of 91% after 4 h of visible light irradiation[97].

In addition, the strong oxidant, O_2 has also been proven to be viable for the production of oxygenate compounds[98-100]. For example, Kalieguine et al. reported VO_x/SiO_2 and TiO_2 photocatalysts for CH_4 conversion into methanol[98]. The reaction was initiated with the C—H bond activation of CH_4 by photogenerated holes-enriched lattice oxygen (O^-). It was demonstrated that methanol could be produced through this reaction condition. Yet, the selectivity of the methanol production was relatively low due to the aforementioned overoxidation problem. Therefore, the suppression of the overoxidation reaction remains a huge challenge in the presence of strong oxidants for the aim of obtaining high oxygenate product selectivity.

With this limitation in mind, Ye and co-workers fabricated a ZnO-Au for suppressing the overoxidation problem during the photocatalytic CH_4 conversion in the presence of O_2 and water[101]. It was discovered that the liquid oxygenate (i.e., methanol and formaldehyde) production rate of 125 μmol · h^{-1} was achieved with selectivity over 95% using ZnO-Au through photocatalytic CH_4 conversion (Fig. 11(a)). Interestingly, they also revealed that the amount of water could have a great influence on the activity and selectivity of CH_4 conversion. Generally, a high yield and selectivity of liquid oxygenates can only be realized in the presence of water. The authors proposed that the role of water is to dilute the liquid products, thereby alleviating the overoxidation of the reactants and simultaneously facilitating the CH_4 conversion toward liquid oxygenates production. Despite the importance of water, the oxygen source for the oxygenate products is O_2, rather than water, as evidenced by isotope labeling experiments (Fig. 11(b)). Furthermore, the hydroperoxyl radicals (·OOH) were produced on the reduction sites (i.e., Au) of ZnO-Au according to radicals trapping test using electron paramagnetic resonance (EPR) investigations. The preferential production of ·OOH can suppress the production of highly reactive superoxide and thus avoid the overoxidation problem. This result is attributed to the combined effect of the strong H abstraction capability and photogenerated electrons accumulation on the Au. Simultaneously, on the oxidation sites (i.e., ZnO), the

CH_4 molecules were oxidized by photogenerated holes, generating ·CH_3. Finally, this generated ·CH_3 can be coupled with ·OOH to produce CH_3OOH, followed by further transformations into methanol and formaldehyde (Fig. 11(c)). Such a work demonstrated that tuning the selective production of the intermediate reactive oxygen species holds the key to preventing the overoxidation of the reactant during the photocatalytic CH_4 conversion.

Similarly, Tang and co-workers reported the ZnO-Au for the photocatalytic CH_4 conversion with the aims of enhancing the liquid oxygenate product selectivity[102]. In their work, the optimized ZnO-Au reached a methanol production rate of 685 μmol · g^{-1} · h^{-1} with a selectivity of propinquity 100% in the presence of water and H_2O_2 (Fig. 11(d)). In contrast to the previous work, they revealed that ·OOH (-0.046 V $vs.$ NHE), which required high energy input to be produced, was not presented in their system due to the use of low power light source during the reaction (Fig. 11(e)). Therefore, ·OH, which was produced through the oxidation of water and decomposition of H_2O_2, was dominated during the reaction. Specifically, CH_4 was first activated by ·OH to generate ·CH_3. Then these ·CH_3 were coupled with the ·OH to produce methanol (Fig. 11(f)). Despite the excellent performance achieved by ZnO-based photocatalysts in the conversion of methane to oxygenate products, the ZnO in aqueous solutions suffered from the severe photo-corrosion problem under light irradiation. Further efforts should be devoted to improving the stability of ZnO to achieve practical applications.

4.6 Other reactions

In addition to the above-mentioned CH_4 conversion reactions, CH_4 can also be photocatalytically transformed into numerous other products, such as aldehyde, ethanol, acetic acid, acetone, and amino acids (Tab. 1, Entry 11 ~ 17). In comparison with the previously mentioned CH_4 conversion reactions, the production mechanism of these products remains ambiguous due to their relatively complex reaction. For example, Du et al. fabricated a series of ceria nanoparticles with varied contents of oxygen vacancies by calcining commercial CeO_2 powder at different temperatures for photocatalytic CH_4 conversion (Fig. 12(a))[103]. Generally, the CeO_2 calcinated at 1100 °C, which owns the most abundance of oxygen vacancies and Ce^{III} cations (Fig. 12(b)), achieved the highest ethanol production rate of 11.4 μmol · g^{-1} · h^{-1} with a selectivity of 91.5% at ambient conditions (pure water, AM1.5 solar illumination, 25 °C).

Furthermore, Li et al. reported the production of ethylene (C_2H_4) and CO through the CO_2 reforming of
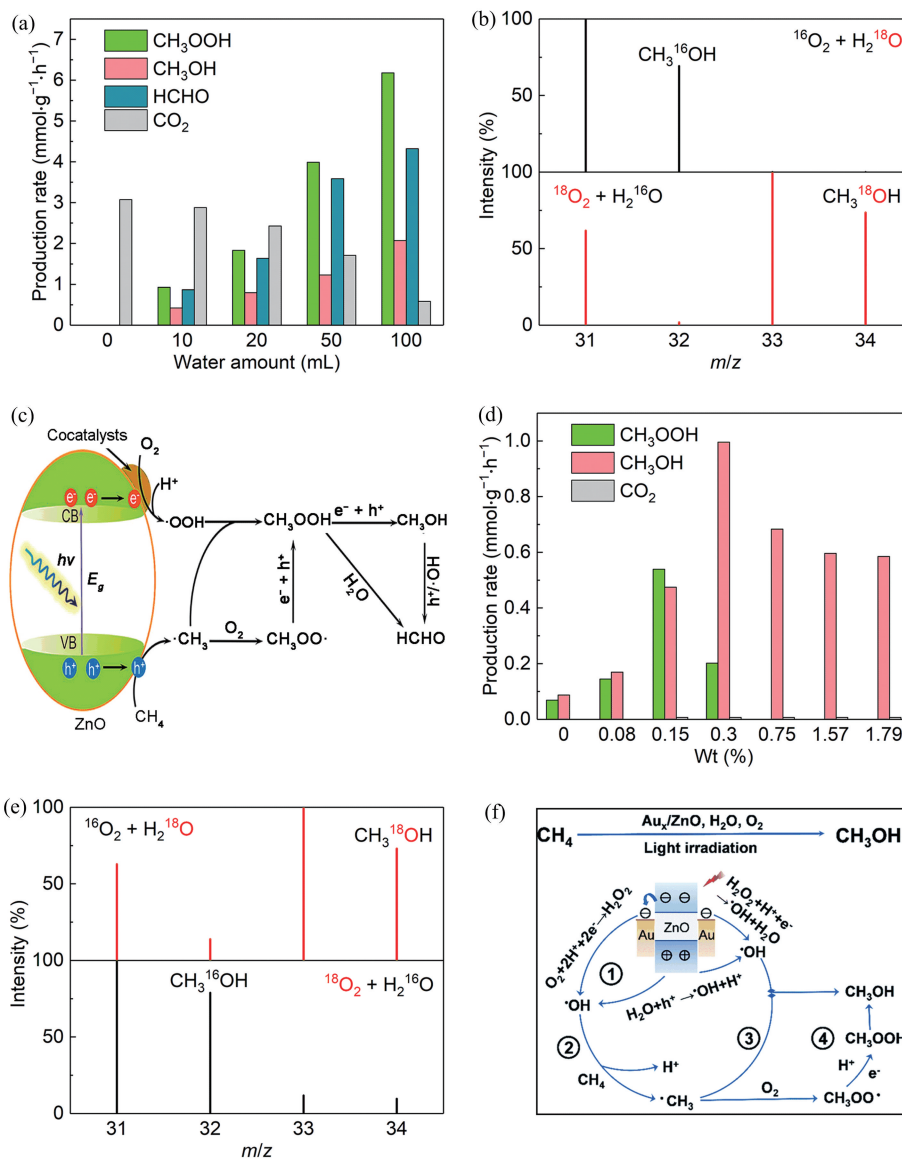
Fig. 11 (a) Comparison of photocatalytic methane conversion performance with the varying H_2O amount over 0.1 wt % Au/ZnO sample under 2 h of light ($300\sim500$ nm) irradiation. (b) GC-MS spectra of CH_3OH produced by photocatalytic conversion of methane under $^{16}O_2$ $+H_2{}^{18}O$ or $^{18}O_2+H_2{}^{16}O$ conditions over 0.1 wt % Au/ZnO. (c) Proposed mechanism for the photocatalytic conversion of methane under O_2+H_2O condition over 0.1 wt % Au/ZnO. (a)$\sim$(c) are Reproduced with permission from Ref.[101]. Copyright 2019, American Chemical Society. (d) Comparison of the photocatalytic methane conversion performance with the O_2+H_2O condition over 0.75 wt % Au/ZnO sample under 2 h of full-spectrum light irradiation. (e) GC-MS spectra of CH_3OH produced by photocatalytic conversion of methane under $^{16}O_2+H_2{}^{18}O$ or $^{18}O_2+H_2{}^{16}O$ conditions over 0.75 wt % Au/ZnO. (f) Proposed mechanism for photocatalytic conversion of methane and O_2+H_2O over 0.75 wt % Au/ZnO. (d)$\sim$(f) are reproduced with permission from Ref.[102]. Copyright 2020, The Royal Society of Chemistry.

CH_4 over noble metal (Ru, Ir, Pd, Rh or Ag)-loaded TiO_2 photocatalysts[106]. Among the metal-TiO_2 composites, the optimized Ag/TiO_2 catalyst delivered the highest C_2H_4 production rate of 686 $\mu mol \cdot g^{-1} \cdot h^{-1}$, accompanied by a CO production rate of 1149 $\mu mol \cdot g^{-1} \cdot h^{-1}$ at a pressure of 2 MPa (Fig. 12(c)). The authors proposed that, upon light irradiation, Ag and TiO_2 were simultaneously photoexcited and the hot electrons transferred from Ag to TiO_2. Then CH_4 and

CO_2 were oxidized by photogenerated holes on Ag and reduced by electrons on TiO_2, respectively, leading to the formation of C_2H_4 and CO (Fig. 12(d)).

Although the products discussed in this section are more valuable than those discussed in the previous sections (i.e., CO_2, CO, C_2H_6 and CH_3OH), the detailed production mechanism of these products remains ambiguous because of their complex reaction pathways involving multiple dehydrogenation and C—C coupling
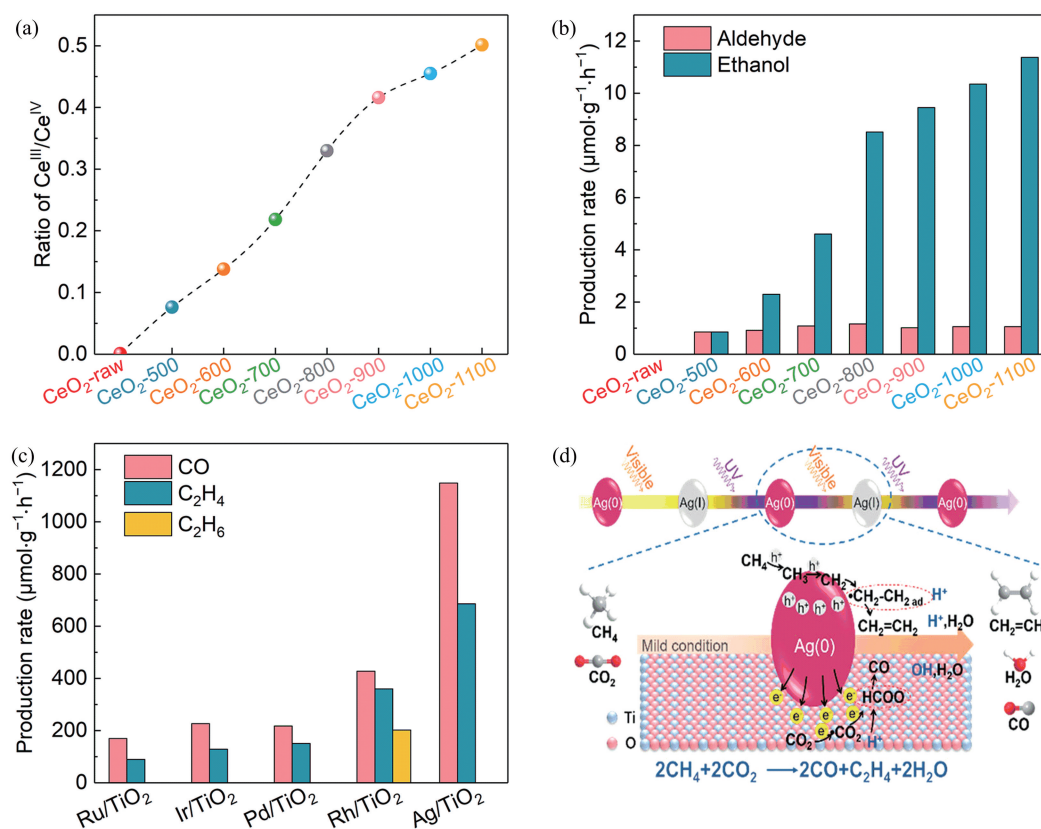
Fig. 12 (a) Ratios of Ce^{III}/Ce^{IV} for CeO_2-raw calcined at different temperatures including 500 °C (CeO_2-500), 600 °C (CeO_2-600), 700 °C (CeO_2-700), 800 °C (CeO_2-800), 900 °C (CeO_2-900), 1000 °C (CeO_2-1000) and 1100 °C (CeO_2-1100). (b) Comparison of the photocatalytic performance of the CeO_2-raw calcined at different temperatures toward aldehyde and ethanol production under 2 h of AM1.5 simulated light irradiation. (a) and (b) are reproduced with permission from Ref. [103]. Copyright 2020, Catalysts. (c) Comparison for the photocatalytic methane conversion performance of the Ru, Ir, Pd, Rh and Ag loaded TiO_2 under simulated solar irradiation. (d) Proposed mechanism for photocatalytic conversion of methane under $CO_2 + H_2O$ condition over Ag/TiO_2. (c) and (d) are reproduced with permission from Ref.[106]. Copyright 2019, American Chemical Society.

reactions. Therefore, further investigation of the formation mechanism for the products discussed in this section must be carried out through various advanced *in situ*/*operando* characterization techniques.

5 Summary and outlook

In summary, metal oxides stand as a class of very promising photocatalysts for CH_4 conversion. In the past two decades, tremendous efforts have been devoted to the studies of metal oxides in this emerging catalytic reaction (see Tab. 2). In this review, we have featured the recent development of the metal oxides in the photocatalytic CH_4 conversion from the viewpoints of fundamental principles and applications. This review is expected to give a concise overview of the metal oxides for photocatalytic CH_4 conversion with a special focus on the roles and functions of metal oxides. Although remarkable progress has been recently achieved in photocatalytic CH_4 conversion by utilizing metal oxides, it remains a great challenge to meet its practical requirements.

Firstly, further enhancing photocatalytic performance is

necessary to achieve its widespread applications. In this regard, continuous efforts should be devoted to manipulating physicochemical properties of metal oxide-based photocatalysts, especially their photogenerated charge carrier utilization efficiency, light absorption ability and surface reactivity, for maximizing their unique advantages in CH_4 conversion photocatalysts. Secondly, achieving selective CH_4 conversion to high value-added multi-carbon products is highly desirable. Overoxidation is the main problem that drives the product selectivity toward low-value CO and CO_2. Thus the control of the oxidation degree of the reactant during photocatalytic CH_4 oxidation using metal oxides should be paid extra attention. To this end, the interaction between reaction intermediates and active sites should be finely tuned to achieve specific functions, such as realizing C — C coupling in the liquid-phase, promoting reaction intermediate dehydrogenation, and suppressing overoxidation. Thirdly, the transformation process of CH_4 on the photocatalyst surface remains ambiguous

Tab. 2 Photocatalytic methane conversion performance of some selected metal oxides and their roles in enhancing the methane conversion efficiency. O: oxidation ability. M: metal-methyl interaction. L: lattice oxygen reactivity.

Photocatalyst	Role of metal oxide	Products	Reaction conditions	Ref.
(Zn^+, Zn^{2+})-ZSM-5$^-$	O, M	C_2H_6, 4.9 μmol $\cdot$ g^{-1} $\cdot$ h^{-1}, >99% H_2, 4.9 μmol $\cdot$ g^{-1} $\cdot$ h^{-1}	[a]RT, 16 h, 1 g, high-pressure Hg-lamp 1000 μmol CH_4 in 25 mL reactor	[21]
Au/m-ZnO-4.8	O, M	C_2H_6, 11.4 μmol $\cdot$ g^{-1} $\cdot$ h^{-1}, >99% H_2, 9.9 μmol $\cdot$ g^{-1} $\cdot$ h^{-1}	RT, 4 h, 1 mg, 300 W Xe lamp 22.3 μmol CH_4 in 40 mL reactor	[78]
Pt-HGTS (2%)	O, M	C_2H_6, 1.3 μmol $\cdot$ g^{-1} $\cdot$ h^{-1}, 90% H_2, 2.1 μmol $\cdot$ g^{-1} $\cdot$ h^{-1}	60 °C, 4 h, 0.2 g, 300 W Xe lamp 44.6 μmol CH_4 in 45 mL reactor	[77]
$Cu_{0.1}Pt_{0.5}$/PC-50	O	C_2 compounds$_{(C2H4+C2H6)}$, 68 μmol $\cdot$ g^{-1} $\cdot$ h^{-1}, 60%	40 °C, 0.1 g, 365 nm LED [b]GHSV = 2400 h^{-1}, O_2/CH_4 = 1:400	[45]
Ga-ETS-10-0.2	O, M, L	C_2H_6, 10.9 μmol $\cdot$ g^{-1} $\cdot$ h^{-1}, >70% Sel$_{C2\text{-}C4}$ > 99%	RT, 0.2 g, high-pressure Hg-lamp 5 h, 200 μmol CH_4 in 20 mL reactor	[83]
Ag-HPW/TiO_2	O, L	C_2H_6, 20.5 μmol $\cdot$ g^{-1} $\cdot$ h^{-1}, 82%	RT, 7 h, 0.1 g, 400 W Xe lamp 0.3 MPa CH_4	[26]
Zn-HPW/TiO_2	O, M, L	CO, 429 μmol $\cdot$ g^{-1} $\cdot$ h^{-1}, 84%	RT, 6 h, 0.1 g, 400 W Xe lamp 0.3 MPa CH_4, 0.1 MPa air	[72]
0.03 wt % Rh/$K_2Ti_6O_{13}$	O	CO_2: 28.8 μmol $\cdot$ g^{-1} $\cdot$ h^{-1}, >99% H_2: 112.5 μmol $\cdot$ g^{-1} $\cdot$ h^{-1}	50 °C, 300 W Xe lamp, 40 mL min^{-1}, 0.8 g, H_2O_{vapor}:CH_4:Ar = 1.5:50:48.5	[107]
Rh/$SrTiO_3$	O, L	CO, 55.0 mmol $\cdot$ g^{-1} $\cdot$ h^{-1} H_2, 54.3 mmol $\cdot$ g^{-1} $\cdot$ h^{-1}	[c]300 °C, 5 mg, 150 W Hg-Xe lamp 10 mL min^{-1}, CH_4:CO_2:Ar = 1:1:98	[71]
WO_3/La	O, hydroxyl groups	CH_3OH, 31.3 μmol $\cdot$ g^{-1} $\cdot$ h^{-1}, 47%	55 °C, 2 h, 0.3 g catalysts in 300 ml H_2O UVC-Vis light, 20 vol% methane in He	[92]
0.33_{metal} wt.% FeO_x/TiO_2	O, hydroxyl groups surface state	CH_3OH, 352 μmol $\cdot$ g^{-1} $\cdot$ h^{-1}, 90%	25 °C, 3 h, 10 mg, 300 W Xe lamp 8 μmol H_2O_2 solution, 70 μmol CH_4	[20]
Au-ZnO	O	Oxygenates$_{(CH3OOH+CH3OH+HCHO)}$ 12.5 mmol $\cdot$ g^{-1} $\cdot$ h^{-1}, 95%	25 °C, 300 W Xe lamp, 100 mL H_2O 2 h, 10 mg, 2 MPa CH_4, 0.1 MPa O_2	[101]
0.1 wt.% Ag-ZnO	O, M	CO_2, >97.3% CH_4 conversion	0.5 g, 300 W Xe lamp, 25 mL/min 78.9% N_2, 21.1% O_2, 100 ppm CH_4	[61]

[a] RT: room temperature; [b] GHSV: gas hourly space velocity; [c] 300 °C: autogenerated temperature under light irradiation.

in most conditions. To this context, advanced in situ characterization techniques should be employed to reveal the atomic and electronic structure of the photocatalyst and transformation pathway of CH_4 molecules during the photocatalytic reaction. Moreover, combining theoretical calculations with the advanced characterizations can help understand the photocatalytic CH_4 conversion mechanism. All these mechanistic investigations are anticipated to pave the way for better designing metal oxide photocatalysts toward highly active and selective CH_4 conversion.

In short, the photocatalytic CH_4 conversion remains in its infancy due to its unsatifactory performance and ambiguous conversion mechanism. Fortunately, with the rapid advancement in materials synthesis and characterization techniques, it could be foreseen that the research and development in the metal oxides-based photocatalytic CH_4 conversion will bloom in the near future, accelerating its advancement toward practical applications.

Acknowledgements

Conflict of interest

The authors declare no conflict of interest.

Author information

JIANG Wenbin is currently a graduate student under the tutelage of Prof. Xiong Yujie at University of Science and Technology of China. His research interests focus on controlled synthesis of metal-oxide hybrid nanostructures for catalytic applications and mechanistic investigations. E-mail: jiangwb@ mail.ustc.edu.cn

LOW Jingxiang obtained his Ph.D. degree from Wuhan University of Technology in 2018, and is currently a postdoctoral fellow at University of Science and Technology of China. His research interests focus on photocatalyst design for carbon dioxide reduction, nitrogen fixation and methane conversion.

QIU Chang is currently a senior student majoring in materials chemistry at University of Science and Technology of China. Her current research interest is photocatalysis for methane conversion.

LONG Ran (corresponding author) is an associate professor at University of Science and Technology of China (USTC). She received her B.S. degree in Chemistry in 2009 and Ph.D. degree in Inorganic Chemistry under the tutelage of Prof. Xiong Yujie in 2014, both from USTC. Her research interests focus on controlled synthesis and catalytic applications of metal nanocrystals. So far, she has published more than 70 SCI papers in international high-level academic journals including J. Am. Chem. Soc., Angew. Chem. Int. Ed., Adv. Mater., Chem. Soc. Rev., Nano Energy and Small.

XIONG Yujie (corresponding author) is the Cheung Kong Chair Professor of Chemistry at University of Science and Technology of China (USTC). He received his B.S. degree in Chemical Physics in 2000 and Ph.D. degree in Inorganic Chemistry in 2004, both from USTC. From 2004 to 2009, he worked as a Postdoctoral Fellow at University of Washington in Seattle and as a Research Associate at University of Illinois at Urbana-Champaign, respectively. He was the Principal Scientist of the National Nanotechnology Infrastructure Network (NSF-NNIN) site at Washington University in St. Louis in 2009 ～ 2011, and joined the USTC faculty as a Professor of Chemistry in 2011. His research centers on solar-driven artificial carbon cycle. He has published more than 200 scientific papers with over 25000 total citations (H-index 77), and is among the Highly Cited Researchers by Clarivate Analytics and the Most Cited Chinese Researchers by Elsevier.

References

[1] Schwach P, Pan X, Bao X. Direct conversion of methane to value-added chemicals over heterogeneous catalysts: Challenges and prospects. Chem. Rev., 2017, 117(13): 8497-8520.

[2] Yuliati L, Yoshida H. Photocatalytic conversion of methane. Chem. Soc. Rev., 2008, 37(8): 1592-1602.

[3] Meng X, Cui X, Rajan N P, et al. Direct methane conversion under mild condition by thermo-, electro-, or photocatalysis. Chem, 2019, 5(9): 2296-2325.

[4] Song H, Meng X, Wang Z-J, et al. Solar-energy-mediated methane conversion. Joule, 2019, 3(7): 1606-1636.

[5] Horn R, Schloegl R. Methane activation by heterogeneous catalysis. Catal. Lett., 2015, 145(1): 23-39.

[6] Guo X, Fang G, Li G, et al. Direct, nonoxidative conversion of methane to ethylene, aromatics, and hydrogen. Science, 2014, 344(6184): 616-619.

[7] Jin Z, Wang L, Zuidema E, et al. Hydrophobic zeolite modification for in situ peroxide formation in methane oxidation to methanol. Science, 2020, 367(6474): 193-197.

[8] Agarwal N, Freakley S J, Mcvicker R U, et al. Aqueous Au-Pd colloids catalyze selective CH_4 oxidation to CH_3OH with O_2 under mild conditions. Science, 2017, 358(6360): 223-226.

[9] Liu Z, Huang E, Orozco I, et al. Water-promoted interfacial pathways in methane oxidation to methanol on a CeO_2-Cu_2O catalyst. Science, 2020, 368(6490): 513-517.

[10] Xu Y D, Lin L W. Recent advances in methane dehydro-aromatization over transition metal ion-modified zeolite catalysts under non-oxidative conditions. Appl. Catal. A: Gen., 1999, 188(1/2): 53-67.

[11] Halabi M H, De Croon M H J M, Van Der Schaaf J, et al. Low temperature catalytic methane steam reforming over ceria-zirconia supported rhodium. Appl. Catal. A: Gen., 2010, 389(1/2): 68-79.

[12] Song H, Meng X, Wang Z-J, et al. Visible-light-mediated methane activation for steam methane reforming under mild conditions: a case study of Rh/TiO_2 catalysts. ACS Catal., 2018, 8(8): 7556-7565.

[13] Cui X, Li H, Wang Y, et al. Room-temperature methane conversion by graphene-confined single iron atoms. Chem, 2018, 4(8): 1902-1910.

[14] Ikuno T, Zheng J, Vjunov A, et al. Methane oxidation to methanol catalyzed by Cu-oxo clusters stabilized in NU-1000 metal-organic framework. J. Am. Chem. Soc., 2017, 139(30): 10294-10301.

[15] Upham D C, Agarwal V, Khechfe A, et al. Catalytic molten metals for the direct conversion of methane to hydrogen and separable carbon. Science, 2017, 358(6365): 917-920.

[16] Newton M A, Knorpp A J, Pinar A B, et al. On the mechanism underlying the direct conversion of methane to methanol by copper hosted in zeolites; Braiding Cu K-edge XANES and reactivity studies. J. Am. Chem. Soc., 2018, 140(32): 10090-10093.

[17] Zhu C, Hou S, Hu X, et al. Electrochemical conversion of methane to ethylene in a solid oxide electrolyzer. Nat. Commun., 2019, 10: 1173.

[18] Arnarson L, Schmidt P S, Pandey M, et al. Fundamental limitation of electrocatalytic methane conversion to methanol. Phys. Chem. Chem. Phys., 2018, 20(16): 11152-11159.

[19] Baltrusaitis J, Jansen I, Christus J D S. Renewable energy based catalytic CH_4 conversion to fuels. Catal. Sci. Technol., 2014, 4(8): 2397-2411.

[20] Xie J, Jin R, Li A, et al. Highly selective oxidation of methane to methanol at ambient conditions by titanium dioxide-supported iron species. Nat. Catal., 2018, 1(11): 889-896.

[21] Li L, Li G-D, Yan C, et al. Efficient sunlight-driven dehydrogenative coupling of methane to ethane over a Zn^+-modified zeolite. Angew. Chem. Int. Ed., 2011, 50(36): 8299-8303.

[22] Hu A, Guo J-J, Pan H, et al. Selective functionalization of methane, ethane, and higher alkanes by cerium photocatalysis. Science, 2018, 361(6403): 668-672.

[23] Liu J, Zhang Y-H, Bai Z-M, et al. Photoelectrocatalytic oxidation of methane into methanol and formic acid over ZnO/graphene/polyaniline catalyst. Chin. Phys. B, 2019, 28(4): 048101.

[24] Amano F, Shintani A, Tsurui K, et al. Photoelectrochemical homocoupling of methane under blue light irradiation. ACS Energy Lett., 2019, 4(2): 502-507.

[25] Li W, He D, Hu G, et al. Selective CO production by photoelectrochemical methane oxidation on TiO_2. ACS Cent. Sci., 2018, 4(5): 631-637.

[26] Yu X, Zholobenko V L, Moldovan S, et al. Stoichiometric methane conversion to ethane using photochemical looping at ambient temperature. Nat. Energy., 2020, 5(7): 511-519.

[27] Li L, Fan S, Mu X, et al. Photoinduced conversion of methane into benzene over GaN nanowires. J. Am. Chem. Soc., 2014, 136(22): 7793-7796.

[28] Li N, Li Y, Jiang R, et al. Photocatalytic coupling of methane and CO_2 into C_2-hydrocarbons over Zn doped g-C_3N_4 catalysts. Appl. Surf. Sci., 2019, 498: 143861.

[29] Zhou Y, Zhang L, Wang W. Direct functionalization of methane into ethanol over copper modified polymeric carbon nitride via photocatalysis. Nat. Commun., 2019, 10: 506.

[30] Sankar M, He Q, Engel R V, et al. Role of the support in gold-containing nanoparticles as heterogeneous catalysts. Chem. Rev., 2020, 120(8): 3890-3938.

[31] Fernandez-Garcia M, Martinez-Arias A, Hanson J C, et al. Nanostructured oxides in chemistry: Characterization and properties. Chem. Rev., 2004, 104(9): 4063-4104.

[32] Kattel S, Ramirez P J, Chen J G, et al. Active sites for CO_2 hydrogenation to methanol on Cu/ZnO catalysts. Science, 2017, 355(6331): 1296-1299.

[33] Rodriguez J A, Liu P, Stacchiola D J, et al. Hydrogenation of CO_2 to methanol: Importance of metal-oxide and metal-carbide interfaces in the activation of CO_2. ACS Catal., 2015, 5(11): 6696-6706.

[34] Bettahar M M, Costentin G, Savary L, et al. On the partial oxidation of propane and propylene on mixed metal oxide catalysts. Appl. Catal. A: Gen., 1996, 145(1/2): 1-48.

[35] Suchorski Y, Kozlov S M, Bespalov I, et al. The role of metal/oxide interfaces for long-range metal particle activation during CO oxidation. Nature Mater., 2018, 17(6): 519-522.

[36] Derita L, Resasco J, Dai S, et al. Structural evolution of atomically dispersed Pt catalysts dictates reactivity. Nature Mater., 2019, 18(7): 746-751.

[37] Vayssilov G N, Lykhach Y, Migani A, et al. Support nanostructure boosts oxygen transfer to catalytically active platinum nanoparticles. Nature Mater., 2011, 10(4): 310-315.

[38] Fujishima A, Honda K. Electrochemical photolysis of water at a semiconductor electrode. Nature, 1972, 238(5358): 37-38.

[39] Kumar S G, Rao K S R K. Comparison of modification strategies towards enhanced charge carrier separation and photocatalytic degradation activity of metal oxide semiconductors (TiO_2, WO_3 and ZnO). Appl. Surf. Sci., 2017, 391: 124-148.

[40] Zhang N, Li X, Ye H, et al. Oxide defect engineering enables to couple solar energy into oxygen activation. J. Am. Chem. Soc., 2016, 138(28): 8928-8935.

[41] Liu X, Iocozzia J, Wang Y, et al. Noble metal-metal oxide nanohybrids with tailored nanostructures for efficient solar energy conversion, photocatalysis and environmental remediation. Energy Environ. Sci., 2017, 10(2): 402-434.

[42] Wu D, Li Z, Qi Z, et al. Boosting photocatalytic activity in cross-coupling reactions by constructing Pd-oxide heterostructures. ChemNanoMat, 2020, 6(6): 920-924.

[43] Zhang N, Li X, Liu Y, et al. Defective tungsten oxide hydrate nanosheets for boosting aerobic coupling of amines: Synergistic catalysis by oxygen vacancies and bronsted acid sites. Small, 2017, 13(31): 1701354.

[44] Li H, Shang J, Ai Z, et al. Efficient visible light nitrogen fixation with BiOBr nanosheets of oxygen vacancies on the exposed {001} facets. J. Am. Chem. Soc., 2015, 137(19): 6393-6399.

[45] Li X, Xie J, Rao H, et al. Platinum- and CuO_x-decorated TiO_2 photocatalyst for oxidative coupling of methane to C_2 hydrocarbons in a flow reactor. Angew. Chem. Int. Ed., 2020, 59: 19702-19707.

[46] Low J, Yu J, Jaroniec M, et al. Heterojunction photocatalysts. Adv. Mater., 2017, 29(20): 1601694.

[47] Scarano D, Bordiga S, Bertarione S, et al. The IR spectroscopy of methane and hydrogen adsorbed on alpha-chromia. Catal. Lett., 2000, 68(3/4): 185-190.

[48] Scarano D, Bertarione S, Spoto G, et al. FTIR spectroscopy of hydrogen, carbon monoxide, and methane adsorbed and co-adsorbed on zinc oxide. Thin Solid Films, 2001, 400(1/2): 50-

55.

[49] Luzgin M V, Gabrienko A A, Rogov V A, et al. The "Alkyl" and "Carbenium" pathways of methane activation on Ga-modified zeolite BEA: C-13 solid-state NMR and GC-MS study of methane aromatization in the presence of higher alkane. J. Phys. Chem. C, 2010, 114(49): 21555-21561.

[50] Tang Y, Li Y, Fung V, et al. Single rhodium atoms anchored in micropores for efficient transformation of methane under mild conditions. Nat. Commun., 2018, 9: 1231.

[51] Shan J, Li M, Allard L F, et al. Mild oxidation of methane to methanol or acetic acid on supported isolated rhodium catalysts. Nature, 2017, 551(7682): 605-608.

[52] Shimura K, Kato S, Yoshida T, et al. Photocatalytic steam reforming of methane over sodium tantalate. J. Phys. Chem. C, 2010, 114(8): 3493-3503.

[53] Anzai A, Fujiwara K, Yamamoto A, et al. Platinum-loaded lanthanum-doped calcium titanate photocatalysts prepared by a flux method for photocatalytic steam reforming of methane. Catal. Today, 2020, 352: 1-9.

[54] Wei J, Yang J, Wen Z, et al. Efficient photocatalytic oxidation of methane over beta-Ga_2O_3/activated carbon composites. RSC Adv., 2017, 7(60): 37508-37521.

[55] Grcic I, Marcec J, Radetic L, et al. Ammonia and methane oxidation on TiO_2 supported on glass fiber mesh under artificial solar irradiation. Environ. Sci. Pollut. Res., 2020. https://doi.org/10.1007/s11356-020-09561-y .

[56] Pan X, Chen X, Yi Z. Photocatalytic oxidation of methane over $SrCO_3$ decorated $SrTiO_3$ nanocatalysts via a synergistic effect. Phys. Chem. Chem. Phys., 2016, 18(46): 31400-31409.

[57] Zhang W, Yu Y, Yi Z. Controllable synthesis of $SrCO_3$ with different morphologies and their co-catalytic activities for photocatalytic oxidation of hydrocarbon gases over TiO_2. J. Mater. Sci., 2017, 52(9): 5106-5116.

[58] Liang X, Wang P, Gao Y, et al. Design and synthesis of porous M-ZnO/CeO_2 microspheres as efficient plasmonic photocatalysts for nonpolar gaseous molecules oxidation: Insight into the role of oxygen vacancy defects and M = Ag, Au nanoparticles. Appl. Catal. B: Environ., 2020, 260: 118151.

[59] Yang J, Xiao W, Chi X, et al. Solar-driven efficient methane catalytic oxidation over epitaxial $ZnO/La_{0.8}Sr_{0.2}CoO_3$ heterojunctions. Appl. Catal. B: Environ., 2020, 265: 118469.

[60] Wang Z, Feng S, Yang P. Catalytic combustion of methane over double perovskite $Sr_2Fe_{1-x}Mg_xMoO_6$ mixed oxides. J. Univ. Sci. Tech. China, 2010, 40(4): 358-362.

[61] Chen X, Li Y, Pan X, et al. Photocatalytic oxidation of methane over silver decorated zinc oxide nanocatalysts. Nat. Commun., 2016, 7: 12273.

[62] Li Z, Pan X, Yi Z. Photocatalytic oxidation of methane over CuO-decorated ZnO nanocatalysts. J. Mater. Chem. A, 2019, 7(2): 469-475.

[63] Liu H, Meng X, Thang Duy D, et al. Conversion of carbon dioxide by methane reforming under visible-light irradiation: Surface-plasmon-mediated nonpolar molecule activation. Angew. Chem. Int. Ed., 2015, 54(39): 11545-11549.

[64] Han B, Wei W, Chang L, et al. Efficient visible light photocatalytic CO_2 reforming of CH_4. ACS Catal., 2016, 6(2): 494-497.

[65] Liu H, Song H, Zhou W, et al. A promising application of optical hexagonal TaN in photocatalytic reactions. Angew.

Chem. Int. Ed., 2018, 57(51): 16781-16784.

[66] Pakhare D, Spivey J. A review of dry (CO_2) reforming of methane over noble metal catalysts. Chem. Soc. Rev., 2014, 43(22): 7813-7837.

[67] Kohno Y, Tanaka T, Funabiki T, et al. Reaction mechanism in the photoreduction of CO_2 with CH_4 over ZrO_2. Phys. Chem. Chem. Phys., 2000, 2(22): 5302-5307.

[68] Teramura K, Tanaka T, Ishikawa H, et al. Photocatalytic reduction of CO_2 to CO in the presence of H_2 or CH_4 as a reductant over MgO. J. Phys. Chem. B, 2004, 108(1): 346-354.

[69] Yuliati L, Itoh H, Yoshida H. Photocatalytic conversion of methane and carbon dioxide over gallium oxide. Chem. Phys. Lett., 2008, 452(1/2/3): 178-182.

[70] Laszlo B, Baan K, Varga E, et al. Photo-induced reactions in the CO_2-methane system on titanate nanotubes modified with Au and Rh nanoparticles. Appl. Catal. B: Environ., 2016, 199: 473-484.

[71] Shoji S, Peng X, Yamaguchi A, et al. Photocatalytic uphill conversion of natural gas beyond the limitation of thermal reaction systems. Nat. Catal., 2020, 3(2): 148-153.

[72] Yu X, De Waele V, Lofberg A, et al. Selective photocatalytic conversion of methane into carbon monoxide over zinc-heteropolyacid-titania nanocomposites. Nat. Commun., 2019, 10: 700.

[73] Yuliati L, Hamajima T, Hattori T, et al. Highly dispersed Ce(III) species on silica and alumina as new photocatalysts for non-oxidative direct methane coupling. Chem. Commun., 2005, (38): 4824-4826.

[74] Yuliati L, Hamajima T, Hattori T, et al. Nonoxidative coupling of methane over supported ceria photocatalysts. J. Phys. Chem. C, 2008, 112(18): 7223-7232.

[75] Yuliati L, Hattori T, Itoh H, et al. Photocatalytic nonoxidative coupling of methane on gallium oxide and silica-supported gallium oxide. J. Catal., 2008, 257(2): 396-402.

[76] Yoshida H, Matsushita N, Kato Y, et al. Synergistic active sites on SiO_2-Al_2O_3-TiO_2 photocatalysts for direct methane coupling. J. Phys. Chem. B, 2003, 107(33): 8355-8362.

[77] Wu S, Tan X, Lei J, et al. Ga-Doped and Pt-Loaded porous TiO_2-SiO_2 for photocatalytic nonoxidative coupling of methane. J. Am. Chem. Soc., 2019, 141(16): 6592-6600.

[78] Meng L, Chen Z, Ma Z, et al. Gold plasmon-induced photocatalytic dehydrogenative coupling of methane to ethane on polar oxide surfaces. Energy Environ. Sci., 2018, 11(2): 294-298.

[79] Yu L, Shao Y, Li D. Direct combination of hydrogen evolution from water and methane conversion in a photocatalytic system over Pt/TiO_2. Appl. Catal. B: Environ., 2017, 204: 216-223.

[80] Yu L, Li D. Photocatalytic methane conversion coupled with hydrogen evolution from water over Pd/TiO_2. Catal. Sci. Technol., 2017, 7(3): 635-640.

[81] Zavyalova U, Holena M, Schloegl R, et al. Statistical analysis of past catalytic data on oxidative methane coupling for new insights into the composition of high-performance catalysts. ChemCatChem, 2011, 3(12): 1935-1947.

[82] Lunsford J H. Catalytic conversion of methane to more useful chemicals and fuels: A challenge for the 21st century. Catal. Today, 2000, 63(2/3/4): 165-174.

[83] Li L, Cai Y-Y, Li G-D, et al. Synergistic effect on the

photoactivation of the methane C–H bond over Ga^{3+}-modified ETS-10. Angew. Chem. Int. Ed., 2012, 51(19): 4702-4706.

[84] Mohamedali M, Ayodele O, Ibrahim H. Challenges and prospects for the photocatalytic liquefaction of methane into oxygenated hydrocarbons. Renew. Sust. Energ. Rev., 2020, 131: 110024.

[85] Gondal M A, Hameed A, Yamani Z H, et al. Photocatalytic transformation of methane into methanol under UV laser irradiation over WO_3, TiO_2 and NiO catalysts. Chem. Phys. Lett., 2004, 392(4/5/6): 372-377.

[86] Hameed A, Ismail I M I, Aslam M, et al. Photocatalytic conversion of methane into methanol: Performance of silver impregnated WO_3. Appl. Catal. A: Gen., 2014, 470: 327-335.

[87] Murcia-Lopez S, Villa K, Andreu T, et al. Partial oxidation of methane to methanol using bismuth-based photocatalysts. ACS Catal., 2014, 4(9): 3013-3019.

[88] Murcia-Lopez S, Villa K, Andreu T, et al. Improved selectivity for partial oxidation of methane to methanol in the presence of nitrite ions and $BiVO_4$ photocatalyst. Chem. Commun., 2015, 51(33): 7249-7252.

[89] Noceti R P, Taylor C E, Deste J R. Photocatalytic conversion of methane. Catal. Today, 1997, 33(1/2/3): 199-204.

[90] Taylor C E, Noceti R P. New developments in the photocatalytic conversion of methane to methanol. Catal. Today, 2000, 55(3): 259-267.

[91] Villa K, Murcia-Lopez S, Andreu T, et al. Mesoporous WO_3 photocatalyst for the partial oxidation of methane to methanol using electron scavengers. Appl. Catal. B: Environ., 2015, 163: 150-155.

[92] Villa K, Murcia-Lopez S, Ramon Morante J, et al. An insight on the role of La in mesoporous WO_3 for the photocatalytic conversion of methane into methanol. Appl. Catal. B: Environ., 2016, 187: 30-36.

[93] Villa K, Murcia-Lopez S, Andreu T, et al. On the role of WO_3 surface hydroxyl groups for the photocatalytic partial oxidation of methane to methanol. Catal. Commun., 2015, 58: 200-203.

[94] Murcia-Lopez S, Bacariza M C, Villa K, et al. Controlled photocatalytic oxidation of methane to methanol through surface modification of beta zeolites. ACS Catal., 2017, 7(4): 2878-2885.

[95] Zhu W, Shen M, Fan G, et al. Facet-dependent enhancement in the activity of bismuth vanadate microcrystals for the photocatalytic conversion of methane to methanol. ACS Appl. Nano. Mater., 2018, 1(12): 6683-6691.

[96] Zeng Y, Liu H C, Wang J S, et al. Synergistic photocatalysis-Fenton reaction for selective conversion of methane to methanol at room temperature. Catal. Sci. Technol., 2020, 10(8): 2329-2332.

[97] Yang J, Hao J, Wei J, et al. Visible-light-driven selective oxidation of methane to methanol on amorphous FeOOH coupled m-WO_3. Fuel, 2020, 266: 117104.

[98] Kaliaguine S L, Shelimov B N, Kazansky V B. Reactions of methane and ethane with hole centers O^-. J. Catal., 1978, 55(3): 384-393.

[99] Ward M D, Brazdil J F, Mehandru S P, et al. Methane photoactivation on copper molybdate: An experimental and theoretical study. J. Phys. Chem., 1987, 91(26): 6515-6521.

[100] Li Y, Li J, Zhang G, et al. Selective photocatalytic oxidation of low concentration methane over graphitic carbon nitride-decorated tungsten bronze cesium. ACS Sustain. Chem. Eng., 2019, 7(4): 4382-4389.

[101] Song H, Meng X, Wang S, et al. Direct and selective photocatalytic oxidation of CH_4 to oxygenates with O_2 on cocatalysts/ZnO at room temperature in water. J. Am. Chem. Soc., 2019, 141(51): 20507-20515.

[102] Zhou W, Qiu X, Jiang Y, et al. Highly selective aerobic oxidation of methane to methanol over gold decorated zinc oxideviaphotocatalysis. J. Mater. Chem. A, 2020, 8(26): 13277-13284.

[103] Du J, Chen W, Wu G, et al. Evoked methane photocatalytic conversion to C_2 oxygenates over ceria with oxygen vacancy. Catalysts, 2020, 10(2): 196-206.

[104] Shi D X, Feng Y Q, Zhong S H. Photocatalytic conversion of CH_4 and CO_2 to oxygenated compounds over Cu/CdS-TiO_2/SiO_2 catalyst. Catal. Today, 2004, 98(4): 505-509.

[105] Reiche H, Bard A J. Heterogeneous photosynthetic production of amino acids from methane-ammonia-water at platinum/titanium dioxide. Implications in chemical evolution. J. Am. Chem. Soc., 1979, 101(11): 3127-3128.

[106] Li N, Jiang R, Li Y, et al. Plasma-assisted photocatalysis of CH_4 and CO_2 into ethylene. ACS Sustain. Chem. Eng., 2019, 7(13): 11455-11463.

[107] Shimura K, Kawai H, Yoshida T, et al. Bifunctional rhodium cocatalysts for photocatalytic steam reforming of methane over alkaline titanate. ACS Catal., 2012, 2(10): 2126-2134.

基于金属氧化物的光催化甲烷转化：原理、进展与挑战

江文斌[1]，刘敬祥[1]，邱　畅[1]，龙　冉[1*]，熊宇杰[1,2*]

1.中国科学技术大学合肥微尺度物质科学国家研究中心，能源材料化学协同创新中心，
化学与材料科学学院，国家同步辐射实验室，安徽合肥 230026；
2.合肥综合国家科学中心能源实验室，安徽合肥 230031

摘要：随着可燃冰和页岩气开采技术的迅速发展，甲烷的储量逐年增加.因此，甲烷不仅被视为一种清洁能源，同时也被认为是一种可用于生产高附加值化工产品的碳原料.然而，由于甲烷分子具有十分稳定的成键结构，所以传统的甲烷转化技术（尤其是甲烷水汽重整反应）通常需要大量的能量输入.针对这一问题，光催化技术可

以利用具有高能量的光生载流子来打破甲烷转化的热力学势垒,被认为是在温和条件下实现甲烷转化的一种非常具有前景的途径.在光催化甲烷转化领域,金属氧化物基光催化剂已经得到了广泛的研究,这主要归因于它们的强氧化能力.在本文中,我们首先基于光催化甲烷转化反应的基本原理对金属氧化物在该反应中所具备的优势进行了讨论.随后,我们回顾了近年来金属氧化物基光催化剂在目前各类甲烷转化反应中的研究进展,包括甲烷完全氧化(TOM)、甲烷部分氧化(POM)、甲烷干重整(DRM)、甲烷无氧偶联(NOCM)以及晶格氧辅助的甲烷偶联(LOCM)等几类反应.最后,我们对基于金属氧化物的光催化甲烷转化技术所面临的挑战与机遇进行了展望.

关键词: 光催化;甲烷转化;金属氧化物;表面反应;选择性